Journal of Medicinal Chemistry

pubs.acs.org/jmc

Article

Rational Design and Optimization of m^{6}A-RNA Demethylase FTO Inhibitors as Anticancer Agents

Sarah Huff,[‖] Indrasena Reddy Kummetha,[‖] Lingzhi Zhang, Lingling Wang, William Bray, Jiekai Yin, Vanessa Kelley, Yinsheng Wang, and Tariq M. Rana*

Cite This: *J. Med. Chem.* 2022, 65, 10920−10937

Read Online

ACCESS | Metrics & More | Article Recommendations | Supporting Information

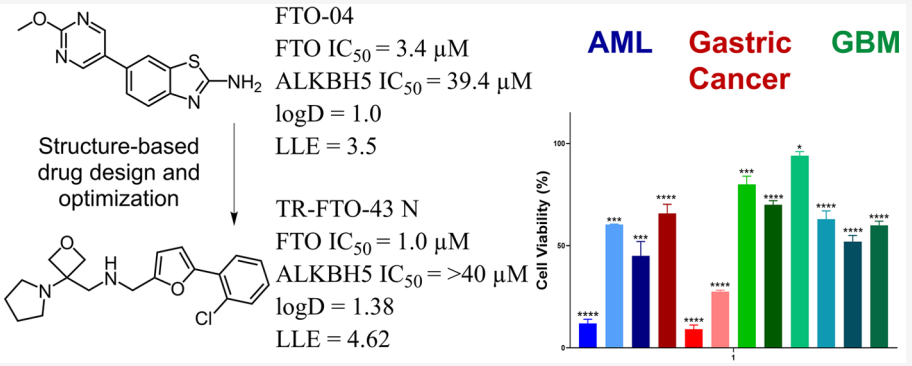

ABSTRACT: Aberrant regulation of N^6-methyladenosine (m^{6}A) RNA modification has been implicated in the progression of multiple diseases, including cancer. Previously, we identified a small molecule inhibitor of the m^{6}A demethylase fat mass- and obesity-associated protein (FTO), which removes both m^{6}A and N^6,2′-*O*-dimethyladenosine (m^{6}A$_m$) RNA modifications. In this work, we describe the rational design and optimization of a new class of FTO inhibitors derived from our previous lead FTO-04 with nanomolar potency and high selectivity against the homologous m^{6}A RNA demethylase ALKBH5. The oxetanyl class of compounds comprise competitive inhibitors of FTO with potent antiproliferative effects in glioblastoma, acute myeloid leukemia, and gastric cancer models where lead FTO-43 demonstrated potency comparable to clinical chemotherapeutic 5-fluorouracil. Furthermore, FTO-43 increased m^{6}A and m^{6}A$_m$ levels in a manner comparable to FTO knockdown in gastric cancer cells and regulated Wnt/PI3K-Akt signaling pathways. The oxetanyl class contains significantly improved anticancer agents with a variety of applications beyond glioblastoma.

INTRODUCTION

N^6-methyladenosine is the most common internal modification in eukaryotic RNA and is known to regulate RNA stability and translation, particularly in mRNAs.[1−4] This dynamic modification is regulated by three classes of proteins, known as "writers", "readers", and "erasers". The multiprotein "writer" complex including METTL3, METTL14, and WTAP installs the methyl modification to mRNAs[5,6] while "reader" proteins, predominantly comprising the YTH domain-containing family (YTHDF1−3 and YTHDC1−2), recognize and bind to the m^{6}A-modified transcripts and mediate downstream signaling events including degradation.[7−10] The "eraser" class of proteins, including both m^{6}A RNA demethylase ALKBH5 (ALKBH5) and fat mass- and obesity-associated protein (FTO), remove the m^{6}A modifications.[11−13] While ALKBH5 has only been demonstrated to recognize and remove m^{6}A methyl groups, FTO is known to also recognize and remove N^6,2′-*O*-dimethyladenosine modifications.[14−18]

After the identification of FTO as an m^{6}A demethylase in 2011, its role in tumorigenesis and poor prognosis of multiple cancers, including GBM and acute myeloid leukemia (AML), has gained widespread interest.[19−29] This interest has led to the identification of several small-molecule inhibitors including rhein, which binds to FTO and its homologue ALKBH5 indiscriminately, and meclofenamic acid (MFA).[30,31] As MFA was identified to increase m^{6}A levels in cells by inhibiting FTO preferentially over ALKBH5, a variety of derivative small-molecule inhibitors were inspired by this structure.[26] One such derivative was recently determined to suppress the proliferation of human-derived AML cell lines in xenotransplanted mice, validating FTO as a druggable cancer target.[26] Interest in the discovery of small molecule inhibitors of FTO is growing

Received: December 7, 2021
Published: August 8, 2022

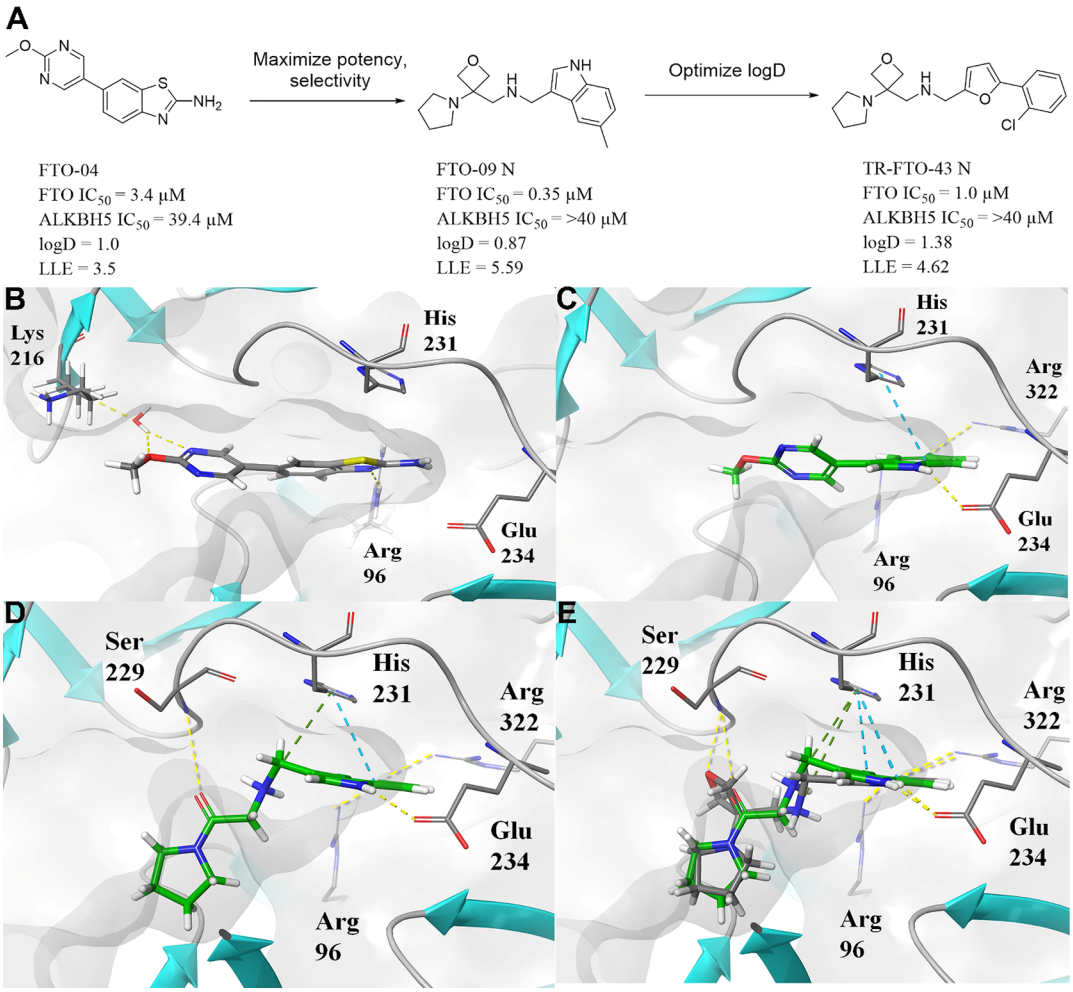

Figure 1. Rational design of oxetanyl FTO inhibitors. (A) Optimization strategy identifying lead FTO-43 N. (B) Docking pose of hit FTO-04. FTO-04 forms a hydrogen bond with Arg 96, and a water-mediated hydrogen bond is observed with Lys 216. Optimization of the benzothiazole ring was directed toward catalytic residues His 231 and Glu 234. (C) Docking pose of FTO-04 with the benzothiazole ring replaced by 5-fluoroindole. New interactions are observed with catalytic His 231, Glu 234, and Arg 322, while interactions are maintained with Arg 96. (D) Docking pose of a pyrrolidine amide replacement of the pyrimidine ring. The amide forms a weak hydrogen bond to the backbone of Ser 229. (E) Comparison of the pyrrolidine amide (green) and oxetane (gray) scaffolds. The oxetane substitution is observed to strengthen the hydrogen bond with Ser 229 without significantly altering the interactions with residues Arg 96, His 231, Glu 234, or Arg 322.

rapidly with the publication of several excellent reviews of existing inhibitors and their applications in 2021.[32,33] However, the cellular efficacy of these analogues is modest, and their use *in vivo* is limited by poor ADME and PK profiles. To progress the development of FTO inhibitors as anticancer therapeutics, it is essential to identify chemically diverse inhibitors with improved cellular efficacy and physicochemical properties.

Recently, we reported the design and biochemical characterization of a novel class of FTO inhibitors with improved physicochemical properties relative to existing inhibitors MFA and FB23-2.[29] Lead compound FTO-04 was determined to inhibit FTO preferentially over its homologue demethylase ALKBH5 with improved potency relative to MFA (Figure 1A). Treatment of glioblastoma stem cell (GSC)-derived neurospheres with FTO-04 resulted in a significant impairment of neurosphere self-renewal and sphere formation, while neurospheres grown from healthy neural stem cells (hNSCs) were not impaired by FTO-04.[29] In this study, we sought to extend our previous work by further optimizing the potency of FTO-04 using a combination of rational design and medicinal chemistry techniques and to broaden the range of applications as a potential chemotherapy.

In this work, we report the identification and characterization of a new class of oxetanyl FTO inhibitors derived from our previous lead FTO-04. This class demonstrated nanomolar potency and high selectivity against the homologue m^6A RNA demethylase ALKBH5 with significantly improved LLE values over FTO-04. We determined that like FTO-04, the oxetanyl class remains to be competitive inhibitors of FTO in agreement with our molecular docking experiments directed at the meclofenamic acid (MA) binding site. This class demonstrated potent antiproliferative effects in a variety of cancer cell models, including glioblastoma, acute myeloid leukemia, and gastric cancer, where FTO is highly upregulated. Lead FTO-43 N was demonstrated to impair growth in multiple gastric cancer cell lines with potency comparable to clinical chemotherapeutic agent 5-fluorouracil and no significant toxicity toward healthy colon cells. Furthermore, FTO-43 N was demonstrated to increase m^6A and m^6A_m levels in a manner comparable to FTO knockdown in gastric cancer cells, confirming that FTO is a relevant cellular target. These data

https://doi.org/10.1021/acs.jmedchem.1c02075
J. Med. Chem. 2022, 65, 10920−10937

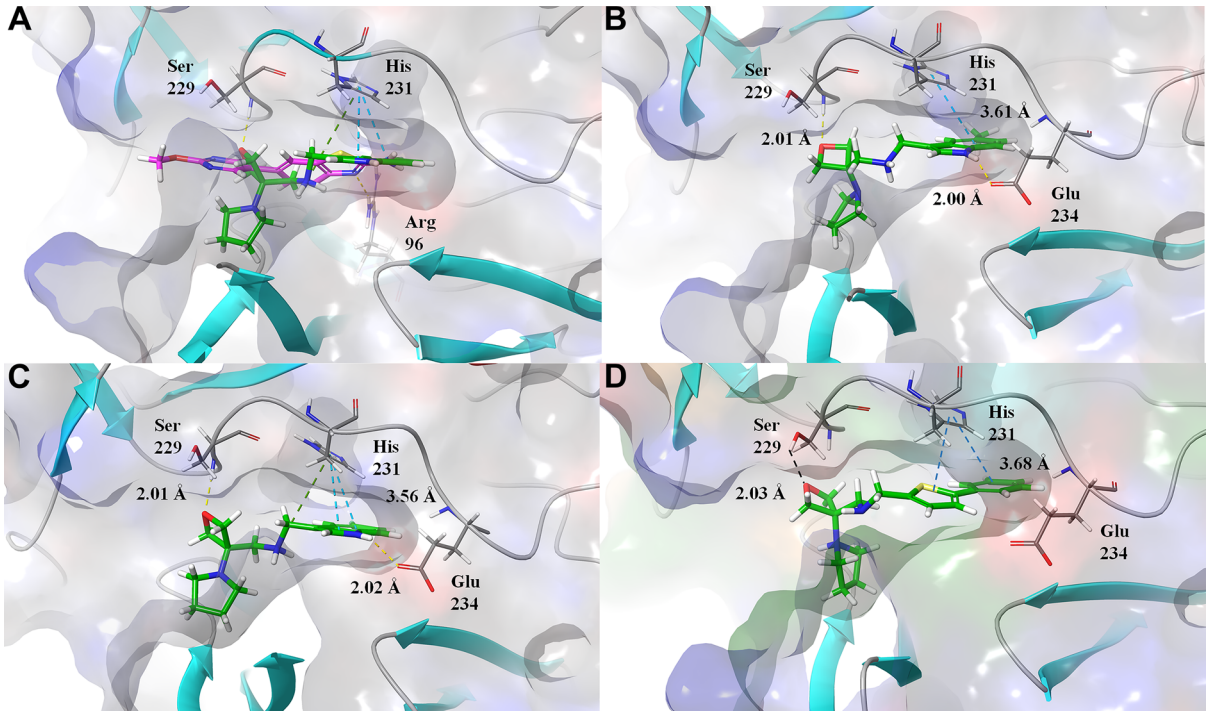

Figure 2. Docking poses for select oxetanyl FTO inhibitors. (A) Optimization strategy. Docking pose of hit FTO-04 with FTO-11 N overlaid. FTO-04 is shown in magenta, and FTO-11 N is shown in green. FTO-04 forms a hydrogen bond with Arg 96 and $\pi-\pi$ interactions with His 231. Optimization sought to strengthen interactions with Ser 229 and Glu 234 while maintaining $\pi-\pi$ interactions with His 231. (B) Docking pose of FTO-09 N. Hydrogen bonds are observed with Ser 229 and Glu 234, and $\pi-\pi$ interactions are observed with His 231. (C) Docking pose of FTO-11 N. Hydrogen bonds are observed with Ser 229 and Glu 234, and $\pi-\pi$ interactions are observed with His 231. (D) Docking pose of FTO-38 N. A hydrogen bond is observed with Ser 229, and $\pi-\pi$ interactions are observed with His 231.

indicate that the oxetanyl class of FTO inhibitors and FTO-43 N specifically are significantly improved antiproliferatives with a variety of applications beyond glioblastoma.

RESULTS

Rational Design and *In Silico* Modeling of Oxetanyl FTO Inhibitors. Previously, we identified a pyrimidine inhibitor that was demonstrated to inhibit FTO competitively with a ~10× preference for FTO over its homologue demethylase ALKBH5. Importantly, FTO-04 exhibited significant impairment of GSC-derived neurosphere formation without impeding neurosphere formation in hNSCs.[29] While this compound presented an interesting lead for optimization, the potency remained modest with an enzymatic IC_{50} of ~3 μM. While FTO-04 showed some selectivity against the homologue ALKBH5 ($IC_{50} \approx 40$ μM), we theorized that selectivity could be further optimized via interactions with the nucleotide recognition lid, which is distinct between FTO and ALKBH5. We therefore sought to improve these parameters using a combination of rational design and medicinal chemistry techniques. Proposed modifications were first docked with Glide XP in the Schrödinger software suite, and compounds were ranked according to their expected docking interactions. Molecular docking was directed toward the catalytic site where we previously predicted FTO-04 would bind.[29] Previous docking indicated FTO-04 was likely to interact with catalytic His 231 and Arg 96 (Figure 1B); in this round of design, we sought to maintain these interactions while forming new interactions with Glu 234 and Ser 229 at the periphery of the binding pocket (Figure 1B–E). Representative docking poses are presented in Figures 1B–E and 2 and Figure S1.

Initial design focused on replacement of the benzothiazole, where a wide variety of heterocyclic and aromatic ring systems were docked to the catalytic site of FTO. Modeling indicated that substituted benzene, pyridine, indole, and biaryl variants were most likely to form favorable interactions with catalytic residues His 231 and Glu 234 while maintaining interactions with Arg 96 (Figure 1C). This modification positioned the pyrimidine ring deeper within the binding pocket such that the expected water-mediated hydrogen bond to Lys 216 observed for FTO-04 is no longer expected. An amine linker was introduced between the ring systems so that interactions with the periphery of the binding site, specifically Ser 229, could be achieved while maintaining the new interactions with His 231 and Glu 234. Subsequent modeling was focused on optimization of the pyrimidine ring, which was modified with a variety of aromatic rings, as well as saturated ring systems intended to introduce more three-dimensional character to the scaffold. Of these, a pyrrolidine amide scaffold was expected to effectively maximize the unoccupied space in the binding pocket and form a hydrogen bond with the amide backbone of Ser 229 (Figure 1D).

In an effort to limit the facile hydrolysis often observed for amide groups, we chose to substitute this feature for an oxetane moiety. Oxetane ring systems have only recently become synthetically feasible groups for drug design, although initial studies indicate that there are several advantages to this system over ketone, ester, and amide variants. Oxetanes are able to form stronger hydrogen bonds than most cyclic ethers and can compete with carbonyl groups as H-bond acceptors. This is due in part to the strained C–O–C bond angle (90.2°, unsubstituted ring) exposing the lone pair electrons and

https://doi.org/10.1021/acs.jmedchem.1c02075
J. Med. Chem. 2022, 65, 10920–10937

Scheme 1. Synthesis of Oxetanyl FTO Inhibitors

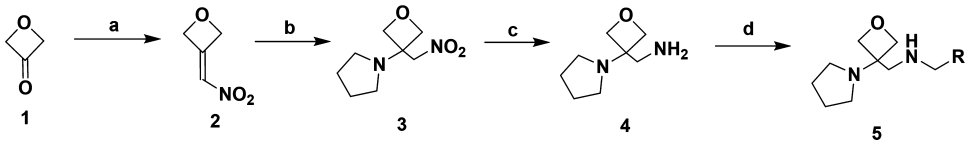

Table 1. *In Vitro* Data Summary for Select Oxetane Inhibitors

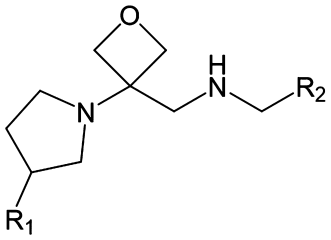

Compound	R_1	R_2	FTO IC_{50} (μM)	ALKBH5 IC_{50} (μM)	elogD	Compound	R_1	R_2	FTO IC_{50} (μM)	ALKBH5 IC_{50} (μM)	elogD
FTO-02 N	H		4.3	19.5	1.02	FTO-39 N	H	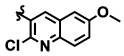	1.7	0.92	1.12
FTO-09 N	H		0.35	>40	0.87	FTO-40 N	H	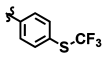	0.16	3.0	1.29
FTO-11 N	H		0.11	6.6	1.01	FTO-41 N	H		2.5	>40	0.85
FTO-12 N	H		0.83	2.3	0.71	FTO-42 N	H		3.0	13.4	0.66
FTO-13 N	H		1.0	>40	0.77	FTO-43 N	H	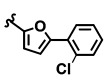	5.5	>40	1.48
FTO-14 N	H		0.87	>40	0.40	FTO-44 N	F		0.44	17.2	0.95
FTO-16 N	H		2.2	0.87	0.70	FTO-45 N	F		0.90	30.5	1.03
FTO-17 N	H		1.3	2.5	0.64	FTO-46 N	F		1.50	>40	0.38
FTO-18 N	H		1.1	41.3	0.71	FTO-47 N	F		2.1	>40	0.38
FTO-27 N	H		0.67	5.9	0.55	FTO-48 N	F	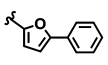	2.0	2.6	1.34
FTO-30 N	H		0.35	9.9	0.87	FTO-49 N	F	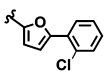	4.0	>40	1.66
FTO-31 N	H		0.95	51.2	1.56	FTO-51 N	H	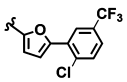	2.0	>40	2.42
FTO-35 N	H	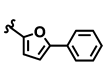	0.07	55.0	1.14	FTO-52 N	H	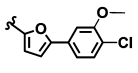	1.3	>40	2.81
FTO-37 N	H		0.81	3.3	0.75	FTO-53 N	H	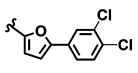	1.3	>40	2.84
FTO-38 N	H	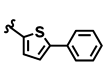	0.27	3.4	1.57						

encouraging H-bond interactions. Replacement of amide groups with oxetanes has been shown to decrease amide basicity and improve chemical stability at a broad pH range (1−10) while maintaining similar dipoles and H-bonding properties.[34−39] Molecular docking of this substituent in place of the proposed amide linker was observed to strengthen the

https://doi.org/10.1021/acs.jmedchem.1c02075
J. Med. Chem. 2022, 65, 10920−10937

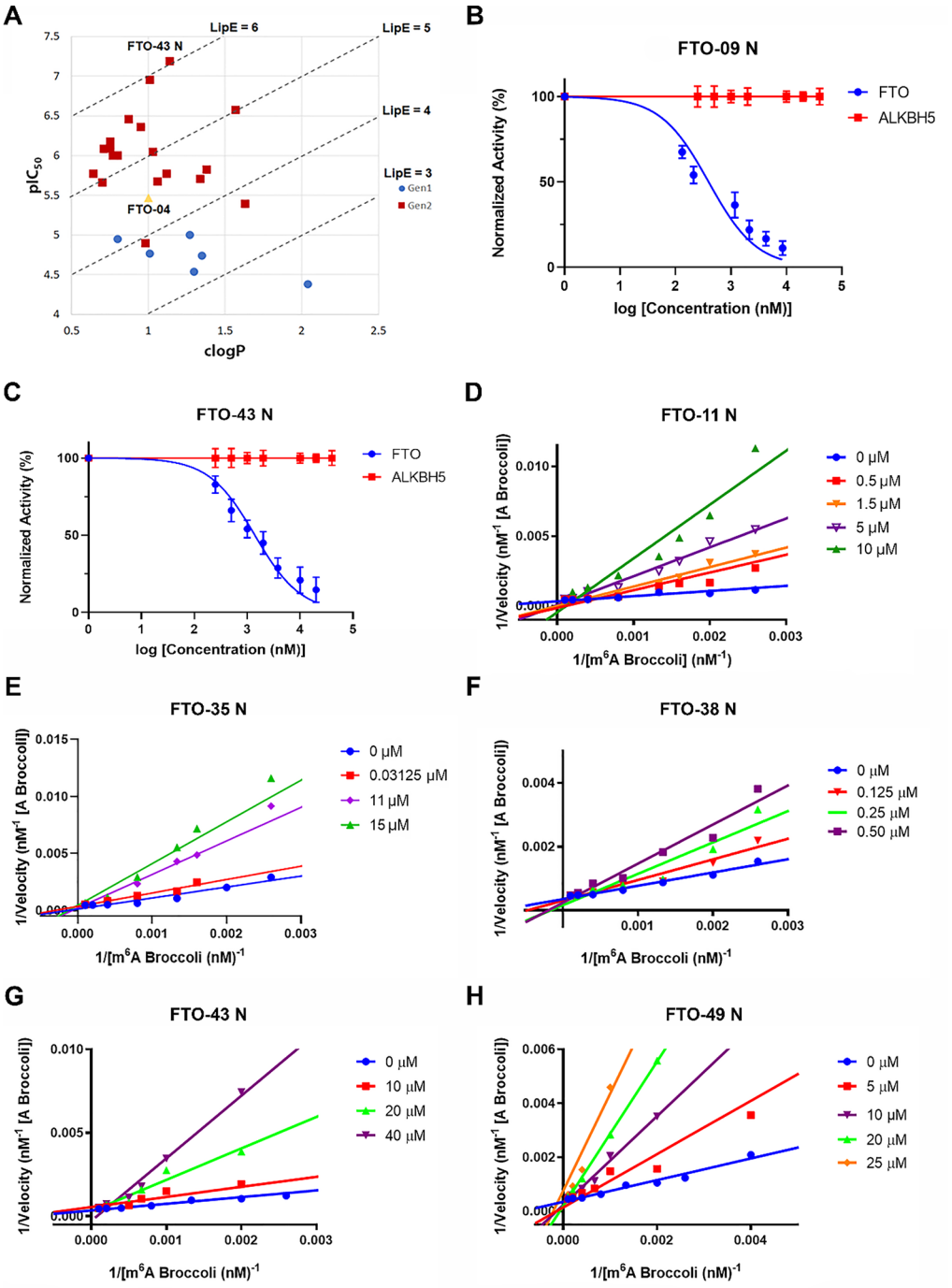

Figure 3. Oxetanyls are potent inhibitors of recombinant FTO in vitro. (A) LLE plot for select FTO inhibitors. pIC_{50} is determined from *in vitro* inhibition assay against recombinant FTO. Oxetanyl libraries (red squares) show a significant improvement in pIC_{50} and LLE from pyrimidine libraries (blue spheres). Hit FTO-04 is shown as a yellow triangle. (B) Dose−response curves for FTO-09 N against recombinant FTO and ALKBH5. (C) Dose−response curves for FTO-43 N against recombinant FTO and ALKBH5. (D) Double-reciprocal plot for FTO-11 N. All data sets converge upon a common *y*-intercept, consistent with competitive inhibition. (E) Double-reciprocal plot for FTO-35 N. All data sets converge upon a common *y*-intercept, consistent with competitive inhibition. (F) Double-reciprocal plot for FTO-38 N. All data sets converge upon a common y-intercept, consistent with competitive inhibition. (G) Double-reciprocal plot for FTO-43 N. All data sets converge upon a common *y*-intercept, consistent with competitive inhibition. (H) Double-reciprocal plot for FTO-49 N. All data sets converge upon a common *y*-intercept, consistent with competitive inhibition.

desired hydrogen bonding interactions with Ser 229 without significantly altering the position of the remainder of the compound scaffold (Figure 1E). As such, we chose to prioritize the oxetanyl pyrrolidine scaffold and focus our *in vitro* evaluation on substitution to the other heterocyclic systems.

Prior to synthesis, physicochemical properties were calculated for each proposed inhibitor using QikProp, including measures of lipophilicity (clogP), membrane permeability (Caco-2 and MDCK model diffusion rates), and solubility (polar surface area and topological polar surface area; Table S1). Preference was given to compounds that were expected to

https://doi.org/10.1021/acs.jmedchem.1c02075
J. Med. Chem. 2022, 65, 10920−10937

show similar physicochemical properties to those observed for clinical candidates with CNS exposure (Table S2);[40−43] however, no compound was excluded from synthesis based on these criteria alone. In total, 53 compounds expected to target the MA binding site with favorable physicochemical properties were selected for synthesis and biochemical evaluation.

Synthesis of the Oxetanyl Library. The synthetic scheme is presented in Scheme 1, where synthesis of the key intermediate **4** was performed as described in McLaughlin *et al.*[39] First, commercially available 3-oxetanone was treated with nitromethane and a catalytic amount of triethylamine to generate a β-nitroalcohol intermediate. Subsequent dehydration with methanesulfonylchloride and excess triethylamine at −78 °C yielded the 3-(nitromethylene)oxetane **2**. Pyrrolidine was coupled to the nitroolefin proceeded with $NaHCO_3$ in THF (**3**), and the nitro group was reduced to a primary amine with Raney Ni under a hydrogen atmosphere to obtain key intermediate **4**. Intermediate **4** was treated with the appropriate aldehyde in methanol to form a Schiff base, which was then reduced by sodium borohydride *in situ* to afford the final product. After extraction with ethyl acetate and water (3 × 15 mL), the crude product was purified by flash column chromatography (MeOH:DCM, 1:9 → 2:8) to afford the final product at >95% purity as determined by analytical HPLC. All compounds were characterized by ^1H and ^{13}C NMR and HRMS prior to biochemical evaluation.

Rationally Designed Oxetanyl Pyrrolidines Inhibit Recombinant FTO with Nanomolar Potency and High Selectivity. To evaluate their ability to inhibit FTO, the compounds were screened against recombinant FTO using the high-throughput fluorescence-based inhibition assay developed by Svensen *et al.*[44] and previously described in Huff *et al.*[29] Briefly, a nonfluorescent methylated RNA substrate termed "m^6A_7-Broccoli" is incubated with FTO in the presence of 2-oxoglutarate (300 μM), $(NH_4)_2Fe(SO_4)_2{\cdot}6H_2O$ (300 μM), and L-ascorbate (2 mM) for 2 h at room temperature in reaction buffer (50 mM NaHEPES (pH 6)). Read buffer (250 mM NaHEPES (pH 9), 1 M KCl, and 40 mM $MgCl_2$) containing the small molecule 3,5-difluoro-4-hydroxybenzylidene imidazolinone (DFHBI-1 T, 2.2 μM) was added to the reaction mixture, and DFHBI-1 T binds preferentially to demethylated Broccoli to produce a fluorescent signal after incubation for 2 h at room temperature. The enzymatic activity of FTO was tested at six concentrations of each inhibitor, ranging from 0−40 μM in triplicate. To exclude false positives, the assays were repeated with demethylated Broccoli to ensure that any change in fluorescence was not due to interference with the A_7 Broccoli-DHBI-1 T complex (Figure S2); no compounds were observed to significantly alter fluorescence signal at concentrations up to 40 μM. Previously, we determined that DMSO does not impair enzyme activity until the concentrations exceed 1% total volume;[29] hence, all inhibitors were dissolved in assay buffer to a final concentration of less than 0.2% DMSO.

The IC_{50} values of the oxetane compounds ranged from 0.07 to >20 μM (Table 1 and Table S1). Approximately half of the compounds showed IC_{50} values below 5 μM, and 11 exhibited submicromolar IC_{50}s. The 30 most potent inhibitors were also screened against ALKBH5 to determine if the compounds showed specificity toward either homologue (Table 1).

Representative dose−response curves are presented in Figure 3B,C. Of these, three showed >10× greater potency toward FTO than ALKBH5 (FTO-09, 11, 13, 14, 18, 30, 31, 35, 38, 40, 44, 45, and 47 N). Four compounds, FTO-09, 13, 14, and 47 N exhibited no inhibition toward ALKBH5 at any concentration tested. Seven compounds showed equivalent potency toward either homologue (defined as <5× difference in IC_{50}; FTO-12, 16, 17, 37, 39, 42, and 48 N).

An examination of fluoroindole substituents revealed that the specificity of the inhibitors is highly dependent on the ring localization of the substituent. FTO-11 N, where the fluorine atom is located on the 5-position of the ring, showed a strong preference toward FTO inhibition relative to ALKBH5 (0.11 μM vs 6.6 μM). However, moving the fluorine atom to either the 3, 4, or 6 position of the indole ring resulted in equivalent IC_{50}s between the two homologues (FTO-12, 16, and 17 N). The docking poses for these compounds indicate that while they are expected to occupy the same region in the binding pocket, placement of the 5-fluoroindole variant binds within hydrogen bonding distance of two arginine residues Arg 96 and Arg 322 (Figure S3). As the fluorine substituent is oriented further away from these residues, the potency against FTO is observed to decrease and any specificity relative to ALKBH5 is lost. Similarly, the 5-methylindole variant FTO-09 N showed no inhibition against ALKBH5 at any concentration tested while inhibiting FTO with submicromolar potency (Table 1). Shifting the methyl group to the 4-position (FTO-42 N) led to a decrease in potency against FTO and a loss of specificity against ALKBH5. The 6-methylindole FTO-18 N, however, retained its selectivity toward FTO, although this substitution was less potent that the 5-methylindole variant.

The Improved Potency of Oxetanyl Inhibitors Is Not Dependent on Increasing Lipophilicity. As part of our optimization strategy, the log*D* and lipophilic ligand efficiency were determined for the 30 most potent and selective inhibitors. We theorized that compounds exhibiting improved potency with modest alterations in lipophilicity were more likely to show adequate solubility properties for cellular and *in vivo* studies. The log*D* was measured for the 30 most potent compounds (Table 1). The log*D* value for previously reported lead compound FTO-04 was also determined for comparison. Figure 3A shows the ligand trajectory plot, where the elogD of the 20 most potent compounds is plotted against the pc as determined by the *in vitro* inhibition assay against recombinant FTO (red squares). For comparison, seven of the most potent compounds from our previous pyrimidine library are included as blue spheres. FTO-04 is included as a yellow triangle. In general, the oxetane class of inhibitors displayed significantly higher pIC_{50}s with average log*D* values similar to lead FTO-04 (log*D* = 1.0). Of the 30 compounds evaluated, 15 compounds showed log*D* <1, and 15 returned a log*D* of <1. Of these, 14 were within the range of 1−3. Compounds with a pIC_{50} of >6 were clustered between log*D* 0.71 and 1.57. These data demonstrate that the optimization of the oxetanyl inhibitors was achieved with minimal increases to lipophilicity and the majority of this class is likely to show favorable solubility properties.

The Oxetanyl Class Is a Competitive Inhibitor of Recombinant FTO. Previously, lead inhibitor FTO-04 was determined to inhibit FTO through a competitive mechanism.[29] To determine if the oxetane class of FTO inhibitors also follows a competitive mechanism, five representative oxetanes were chosen for analysis by steady-state enzyme kinetics. The reaction velocity was determined for FTO in the presence of varying concentrations of FTO-11, 35, 38, 43, and

https://doi.org/10.1021/acs.jmedchem.1c02075
J. Med. Chem. 2022, 65, 10920−10937

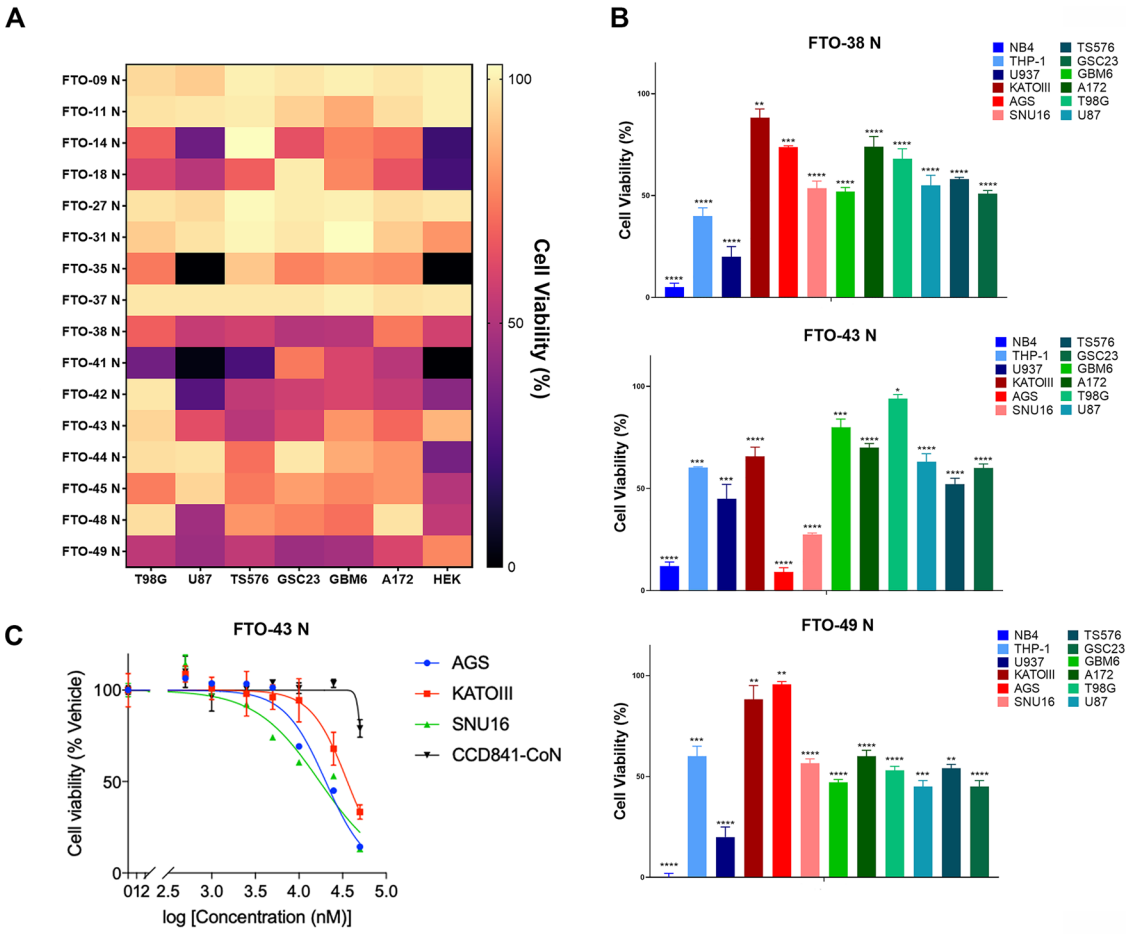

Figure 4. Oxetanyls impair proliferation in multiple cancer subtypes. (A) Heat map depicting the antiproliferative effects of 16 oxetanyl inhibitors in glioblastoma (T98G, U87, TS576, GSC23, GBM6, and A172) and HEK cells. Color indicates cell viability normalized to DMSO control. All cells were treated with a single dose of 30 μM. Cell viability was recorded by MTS assay after 48 h exposure. (B) Single-dose screen (30 μM) of FTO-38 N, FTO-43 N, and FTO-49 N in a broad panel of cancer cells. FTO-43 N shows significant inhibition of AML and gastric cancer subtypes. Cell viability was recorded by MTS assay after 48 h exposure. $N > 10$, $^{*}p < 0.05$, $^{**}p < 0.01$, $^{***}p < 0.001$ by Student's t test. (C) Dose−response curves for FTO-43 N in gastric cancer (AGS, SNU16, and KATOIII) and healthy colon (CCD841) cell lines.

49 N with a range of 10 substrate concentrations between 0 and 10 μM. A plot of the reaction velocity versus substrate concentration shows that all concentrations of inhibitors approach a common v_{max} when substrate concentrations exceed 10 μM (Figure S4). The double-reciprocal plots show all concentrations of either FTO-11, 35, 38, 43, or 49 N converge on a common y-intercept, indicating v_{max} is independent of the concentration of inhibitor, supporting a competitive mechanism of inhibition (Figure 3D−H). This mechanism is consistent with the *in silico* modeling targeted toward the MA binding site and the competitive mechanism previously reported for both MA and lead compound FTO-04.[29,31]

The Oxetane Class of FTO Inhibitors Is a Potent Antiproliferative in Multiple Cancer Models. The role of m^{6}A dysregulation in cancer progression and therapeutic resistance is still emerging, and FTO has been identified as a potential oncogene in a variety of cancers, including AML and GBM.[23,24,26,27,29,45,46] Several recent reports have also indicated that FTO is overexpressed in gastric cancer tissues versus normal adjacent tissues, and this overexpression is correlated with poor overall survival and progression-free survival rates in patients.[47,48] FTO was also found to promote stem-like characteristics in gastric cancer models and promote lymph node metastasis, while knockdown of FTO impaired proliferation, migration, and invasion of gastric cancer cells *in vitro*.[47] For this study, we elected to evaluate the antiproliferative effects of our oxetanyl inhibitors in all three cancer models.

Initially, the 16 most potent and selective compounds identified by our *in vitro* studies were screened in a panel of GBM and GSC cell lines at a single dose of 30 μM. Compounds were also evaluated in HEK cells to estimate their off-target toxicity. Figure 4A illustrates the effects of oxetane inhibitors as a heat map, where cell viability is presented as a gradient from pale yellow (100% viability) to black (0% viability) (data presented in Table S3). Compounds FTO-38, 43, and 49 N were observed to impair cell viability in the majority of glioblastoma lines tested with minimal effects in HEK cells. Interestingly, these compounds also reported log$D$ values near 1.5. At this stage, FTO-38, 43, and 49 N were chosen for further evaluation, while the remainder of the compounds was triaged.

Having identified the three most promising antiproliferative agents in GBM, we next sought to expand our screen to include AML and gastric cancer models for which FTO is an emerging target. A broad panel of cell lines representing glioblastoma, AML, and gastric cancers were treated with 30

https://doi.org/10.1021/acs.jmedchem.1c02075
J. Med. Chem. 2022, 65, 10920−10937

μM of FTO-38, 43, and 49 N for 48 h, and cell viability was assessed by MTS assay. As observed in Figure 4B, antiproliferative effects are consistently observed in all cancer types. FTO-43 N displayed strong growth inhibition in NB4, AGS, and SNU-16 cell lines. Additionally, FTO-43 N showed significantly less toxicity toward HEK cells than FTO-38 and 49 N, indicating that this compound might have a broader therapeutic index. Therefore, we elected to further evaluate FTO-43 N in both AML and gastric cancer cell models, where this compound was most potent.

To establish the time dependency of inhibition, AGS, KATOIII, and SNU-16 cells were treated with varying doses of FTO-43 N, and the cell viability was assessed at 24, 48, and 72 h post-treatment by Cell Titre Glo. As observed in Figure S5, FTO-43 N showed little cytotoxicity until 48 h post-treatment across AGS, SNU-16, and KATOIII cell lines. While some improvement in antiproliferative effects were observed at 72 h, this increase in growth inhibition was modest relative to that observed after 48 h. As such, the remainder of our cell-based experiments were performed 48 h post-exposure.

To determine the IC_{50}, AGS, KATOIII, and SNU-16 cells were treated with eight doses of FTO-43 N (0, 0.5, 1, 2.5, 5, 10, 25, and 50 μM), and the cell viability was examined (Figure 4C). The experiment was also repeated in CCD841-CoN normal colon cells to estimate the therapeutic index. FTO-43 N was also observed to inhibit the growth of gastric cancer cell lines with EC_{50}s ranging from 17.7 to 35.9 μM, and no significant growth inhibition observed in CCD841-CoN normal colon cells (Table 2). These values are within range

Table 2. EC_{50} Values for FTO-43 and 5FU in Gastric Cancer Cells[a]

	CCD 841	AGS	KATOIII	SNU16
FTO-43	>50	20.3	35.9	17.7
5FU	~218	7.25−22	21.4	6.4

[a]IC_{50} values for 5FU averaged from literature reports.[45,46]

of the reported IC_{50} for clinical chemotherapeutic agent 5-fluorouracil in these cell lines (5FU, Table 2).[49,50] These data indicate that FTO-43 N is capable of impairing proliferation of gastric cancer cells with little cytotoxicity toward normal colon cells.

FTO-43 N Increases m^6A Levels and Regulates Wnt/PI3K-Akt Signaling in Gastric Cancer Cells Comparable to FTO Knockdown. Intracellular inhibition of FTO is known to increase the levels of both m^6A and m^6A_m; Yang *et al.* previously reported that shRNA silencing of FTO in AGS cells led to an observable increase in m^6A levels as observed by dot-blot assays.[48] To determine the effects of FTO-43 N on m^6A modifications, AGS cells were first treated with shControl, shFTO1, or shFTO2 to establish the relative change in m^6A levels due to FTO knockdown (knockdown efficiency presented in Figure S6). Dot-blot assay results showed that as expected, both shFTOs were observed to increase m^6A levels (Figure S7A). Similarly, cells treated with FTO-43 N exhibited significantly elevated levels of m^6A relative to DMSO control, indicating that FTO-43 N is able to alter m^6A mRNA levels, which is consistent with FTO knockdown (Figure S7B).

As an orthogonal assay control, the relative levels of m^6A and m^6A_m were further quantified by high-performance liquid chromatography−tandem mass spectrometry (HPLC−MS/MS/MS) (Figure 5). AGS cells were treated with shControl (NTC or ctrl), shFTO1, DMSO, or FTO-43 N, and the polyadenylated messenger RNA were isolated, decapped, and digested to single nucleosides prior to quantification. As observed in Figure 5A, FTO knockdown by shFTO1 led to increased m^6A and m^6A_m levels in AGS cells relative to shControl. Treatment with FTO-43 N also resulted in augmented m^6A and m^6A_m levels with a larger increase for m^6A_m levels, which is in agreement with FTO inhibition (Figure 5B). While one of our datasets does not show a statistically significant increase in m^6A_m levels post-treatment with FTO-43 N, this is likely due to an outlier in the dataset, and the trend is readily apparent in both replicates.

Furthermore, we investigated the mechanism of FTO-43 N inhibition in gastric cancer by analyzing the Wnt/PI3K-Akt signaling pathways. Previous studies have shown that a reduction of m^6A RNA methylation predicted adverse clinical features of gastric cancer and activated oncogenic Wnt/PI3K-Akt signaling to promote malignant phenotypes of gastric cancer cells.[51]

Increasing the levels of m^6A RNA methylation by FTO knockdown reversed these phenotypical and molecular changes in gastric cancer.[51] As shown in Figure 5C, Wnt (marked by Axin 1 and β-catenin expression) and PI3K-Akt (marked by Ser473-Akt phosphorylation) signaling were downregulated by FTO inhibition by shRNA knockdown in AGS gastric cancer cells. Conversely, the expression of E-cadherin (CDH1) was upregulated when FTO was inhibited. Treatment with FTO-43 N replicated this phenotype of downregulated Wnt/PI3K-Akt signaling. Collectively, these data indicate that FTO is likely a cellular target of FTO-43 N.

DISCUSSION

In this work, we sought to improve upon the previously identified FTO inhibitor FTO-04 by increasing potency and selectivity while maintaining favorable physicochemical properties, such as log*D*. Rational design of the oxetanyl class of compounds identified multiple compounds with nanomolar IC_{50}s against recombinant FTO with little inhibition observed against the homologue demethylase ALKBH5 (IC_{50} > 40 M). Log*D* measurement for the most potent and selective compounds indicated that this optimization was independent of large increases in lipophilicity, suggesting that most of the compounds identified in this study are likely to show favorable solubility properties for further development as antiproliferative agents. This class was further found to inhibit FTO competitively, consistent with our *in silico* modeling, and lead FTO-43 N was demonstrated to increase both m^6A and m^6A_m levels in a manner comparable to FTO knockdown in gastric cancer cells, confirming that FTO is a relevant cellular target. Analysis of the Wnt and PI3K-Akt signaling pathways post-treatment with FTO-43 N demonstrated that this compound downregulated both oncogenic signaling pathways in a manner consistent with FTO knockdown. Collectively, these results indicate a successful optimization of our previous hit and the identification of an improved class of FTO inhibitors.

While the role of FTO as an oncogene in AML has been established, its role in the progression and tumorigenesis of other cancer types is still emerging. In this work, we expanded our evaluation of oxetanyl inhibitors to include glioblastoma, which we previously demonstrated was susceptible to FTO inhibition, and gastric cancer. Currently, there are very few reports regarding the role of FTO in gastric cancer; evaluation of TCGA and GTex datasets indicate that FTO is overex-

https://doi.org/10.1021/acs.jmedchem.1c02075
J. Med. Chem. 2022, 65, 10920−10937

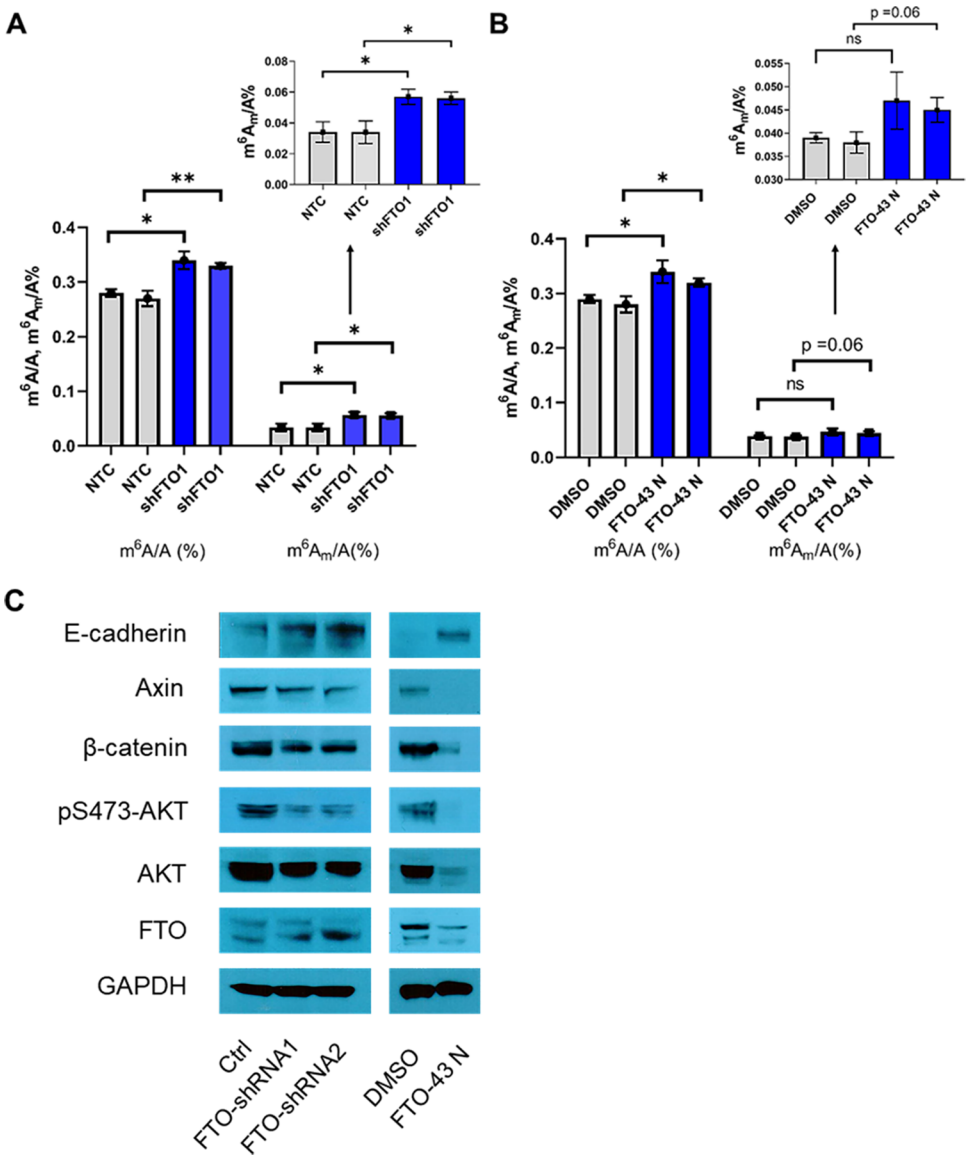

Figure 5. FTO-43 N increases m^6A and m^6A_m levels in gastric cancer cells consistent with FTO knockdown. (A) FTO knockdown by shFTO1 increases both m^6A and m^6A_m levels relative to shNTC control (ctrl or NTC) in AGS gastric cancer cells. (B) Treatment of AGS gastric cancer cells with FTO-43 N increases both m^6A and m^6A_m levels. The data represent the mean ± SEM of duplicate LC−MS/MS measurement results from three biological replicates. The two bars in each data series in (A) and (B) represent results obtained from two separate LC-MS/MS measurements. $*p < 0.05$, $**p < 0.01$, unless otherwise noted, by Student's t test. (C) Western blot analysis of the expression of E-cadherin, Axin1, β-catenin, Akt, Phospho-Akt (Ser473), FTO (top band), and GAPDH. GAPDH served as a loading control.

pressed in gastric cancer tissues versus normal adjacent tissues, and this overexpression is correlated with poor overall survival and progression free survival rates in patients. Xu *et al.* further indicated that FTO expression is correlated with tumor stage, where higher expression was observed in advanced disease stages (clinical stage III and T3−4).[47] Recently, Yang *et al.* reported that FTO stabilized MYC transcripts, leading to overexpression of MYC and accelerated proliferation, invasion, and migration of gastric cancer cells.[48] In our study, we demonstrated that FTO-43 N was able to impair the proliferation of gastric cancer cells with comparable potency to the clinical chemotherapy 5-fluorouracil. These data suggest that FTO inhibition could play a role in gastric cancer progression, although the biological mechanisms for such a role are yet to be established.

Gastric cancer is the fifth most common cancer and the third leading cause of cancer death worldwide. Gastric tumors are highly heterogeneous and resistant to treatments in large part because most cases are diagnosed at advanced stages. Life expectancy for this disease is low with a 5 year survival rate of just 20−30%, and the need for novel methods to target resistant and advanced stage gastric cancers remains urgent. We believe that our data in combination with emerging reports regarding the high upregulation of FTO in gastric cancer suggest further study of the role of FTO in gastric cancer progression is warranted.

While we demonstrate that the oxetanyl class of FTO inhibitors is significantly improved upon our previous hit FTO-04 in accordance with the goals of our study, the applications of these compounds are yet to be fully explored. While FTO-43 N demonstrated antiproliferative effects comparable to the

https://doi.org/10.1021/acs.jmedchem.1c02075
J. Med. Chem. 2022, 65, 10920−10937

clinical chemotherapy 5-fluorouracil in gastric cancer cells, it is important to note that 5-fluorouracil is often administered to patients in combination with other chemotherapies such as cisplatin. Additional studies to evaluate whether FTO-43 N can confer synergistic effects when combined with other FDA-approved chemotherapies would provide vital information regarding the applications of this compound as a potential chemotherapeutic agent. Furthermore, the cell lines used to evaluate FTO-43 N are not enriched in gastric cancer stem cells, where FTO inhibition is most likely to impair cell proliferation and tumorigenesis. Additional studies are warranted to assess FTO-43 N in cancer models with more physiological relevance to the disease stage most likely to respond to FTO inhibition. Nevertheless, we believe that this work presents a successful optimization of our previous hit FTO-04 with many potential antiproliferative applications.

EXPERIMENTAL SECTION

Detailed procedures for *in silico* screening and docking of the inhibitors can be found in the SI. Protocols for protein expression and purification, *in vitro* inhibition assays, and steady-state enzyme kinetics can be found in the SI. Detailed synthetic procedures are presented in the SI. All cell culture procedures can also be found in the SI.

Molecular Modeling with Schrödinger. *In silico* modeling of FTO inhibitors was performed using the Glide docking module of the Schrödinger 11.5 modeling software suite. A crystal structure of FTO bound to meclofenamic acid (MA) (PDB ID: 4QKN)[1] was first refined using Prime.[31,52,53] Missing side chains and hydrogen atoms were resolved before docking, and the Optimized Potentials for Liquid Simulations All-Atom (OPLS) force field and the surface-generalized Born (SGB) continuum solution model was used to optimize and minimize the crystal structures. The docking grid was generated as a 5 Å × 5 Å × 5 Å cube centered on MA. Glycerol and α-ketoglutarate were removed from the docking site prior to grid generation. Ligprep was used to generate a minimized 3D structure for all prospective FTO inhibitors using the OPLS 2001 force field. Docking was performed with Glide XP. QikProp was used to predict physicochemical properties such as clogP and membrane permeability in Caco-2 and MDCK cell lines for the most promising compounds.

Protein Expression and Purification. The protein expression and purification protocol was adapted from Svensen and Jaffrey and previously published in Huff *et al.*[44,29] *Escherichia coli* BL21 competent cells (New England Biolabs) were transformed with a pET28-SUMO-His10-FTO plasmid (a generous gift from the Jaffrey lab) by heat shock and spread on a LB Kanamycin agar plate and then incubated overnight at 37 °C. Two to three colonies were picked and transferred to 5 mL of LB media treated with kanamycin (0.5 mg/mL final concentration) and then grown overnight shaking at 37 °C. The overnight culture was then transferred to 2 L of LB kanamycin medium and incubated at 37 °C until an OD of 0.8 was reached. The culture was cooled at 4 °C for 20 min. induced with 0.5 mM isopropyl β-D-1-thiogalactopyranoside (IPTG), and then grown while shaking at 16 °C. Cell pellets were collected by centrifugation (5000*g* for 10 min at 4 °C), and the supernatant was discarded. The pellets were resuspended in B-PER bacterial protein extraction reagent (6 mL per gram) with DNase 1 (5 U per mL, RNase-free) and incubated at 4 °C for 1 h. The suspension was centrifuged at 10,000*g* for 20 min, and the supernatant was transferred to a Talon Metal Affinity Resin column that had been pre-equilibrized with binding buffer (50 mM NaH_2PO_4 (pH 7.2), 300 mM NaCl, 20 mM imidazole, and 1 mM β-mercaptoethanol in RNase-free water). The supernatant was incubated with the affinity resin column at 4 °C for 1 h with end-over-end rotation. After incubation, the column was washed with 5 bed volumes of binding buffer and then incubated with 1 bed volume of elution buffer (50 mM NaH_2PO_4 (pH 7.2), 300 mM NaCl, 500 mM imidazole, and 5 mM β-mercaptoethanol in RNase-free water) for 20 mins. After incubation, the eluant was collected, and the column was incubated again with 1 bed volume of elution buffer; the elution process was repeated until no further protein was collected (3−5 bed volumes total). The eluant was combined and transferred to a Slyde-A-Lyzer Dialysis Cassette (20,000 MWCO, Thermo Scientific) and dialyzed overnight at 4 °C against dialysis buffer (50 mM Tris−HCl (pH 7.4), 100 mM NaCl, 5 mM B-mercaptoethanol, and 5% (v/v) glycerol in RNase-free water). Protein concentration was measured by absorbance at 280 nm and calculated by Beer−Lambert's Law ($A = \varepsilon/C$, ε_{FTO} = 95,340). ALKBH5 was expressed and purified from pET28-SUMO-His10-ALKBH5 plasmid by the same procedure described above.

***In Vitro* Inhibition Assay Method.** The *in vitro* inhibition assay method was adapted from Svenson and Jaffrey and previously reported in Huff *et al.*[44,29] All reactions were performed in a 96-well plate with 200 μL of assay buffer (50 mM HEPES (pH 6), 300 μM 2-oxoglutarate, 300 μM $(NH_4)_2Fe(SO_4)_2 \cdot 6\ H_2O$, and 2 mM ascorbic acid in RNase-free water) with 7.5 μM m^6A_7-Broccoli RNA and 0.250 μM FTO. Inhibitors were added in concentrations ranging from 0.008 to 40 μM; all inhibitors were dissolved in DMSO and added to a final concentration of 0.2% DMSO. Previously, we demonstrated that FTO activity is stable at concentrations of DMSO up to 1% (v/v).[29] Prior to incubation, 40 μL of read buffer (250 mM HEPES (pH 9.0), 1 M KCl, 40 mM $MgCl_2$, and 2.2 μM DFHBI-1 T in RNase-free water) was added to bring the final well volume to 200 μL. After incubation at room temperature for 2 h, the plates were left at 4 °C overnight (16 h) to allow DFHBI-1 T to bind to A_7-Broccoli RNA. Specificity assays were performed by the same method with 0.250 μM ALKBH5. Fluorescence intensity was measured with a BioTek Synergy plate reader with FITC filters (excitation, 485 nm; emission, 510 nm). Sigmoidal dose−response curves were fitted in GraphPad Prism 8. All assays were performed in triplicate, with additional repetitions added as necessary.

Michealis−Menton kinetics was performed using the inhibition assay procedure described above; the activity of FTO concentrations of 0, 0.250, 0.385. 0.500, 0.625, 0.750, 1.25, 2.5, 5, and 10 μM m^6A Broccoli were recorded for the following concentrations of FTO-11 N: 0, 0.5, 1.5, 5, and 10 μM, and for FTO-35 N: 0, 0.03125, 11, and 15 μM, FTO-38 N: 0, 0.125, 0.25, and 0.5 μM, FTO-43 N: 0, 10, 20, and 40 μM, FTO-49 N: 0, 5, 10, 20, and 25 μM. The data were fitted in GraphPad Prism 8.

*General Synthetic Procedures. Synthesis of 3-(Nitromethylene)-oxetane (**2**).* Synthesis of 3-(nitromethylene)oxetane (**2**) was performed as described in Wuitschik *et al.*[9] and McLaughlin *et al.*[10] 3-Oxetanone (130 μL, 2.03 mmol), nitromethane (154 μL, 2.85 mmol), and NEt_3 (57 μL, 0.41 mmol) were stirred at RT for 30 min and then diluted with CH_2Cl_2 (10 mL) and cooled to −78 °C. To this solution was added NEt_3 (565 μL, 4.05 mmol), followed by MsCl (157 μL, 2.03 mmol) dropwise over 10 min. The reaction mixture was stirred at −78 °C for 40 min. The reaction mixture was allowed to warm to RT and directly poured on a column (15% → 25% EtOAc in hexane), providing compound (**2**) as a yellow oil.

*Synthesis of 1-(3-(Nitromethyl)oxetan-3-yl)pyrrolidine (**3**).* Synthesis of 1-(3-(nitromethyl)oxetan-3-yl)pyrrolidine (**3**) was adapted from procedures described in McLaughlin *et al.*[10]A stirred solution of SM (**2**) (1 eq) in THF was treated with $NaHCO_3$ (1 eq) and pyrrolidine (1 eq) at room temperature. The reaction mixture was stirred for 1 h at room temperature. After completion of the reaction, the reaction mixture was filtered through a Celite bed. The solvent was evaporated under vacuum, and the crude product was purified by column chromatography (EtOH:hexane, 1:9 → 2:8) to give compound (**3**) as a liquid.

*Synthesis of (3-(Pyrrolidin-1-yl)oxetan-3-yl)methanamine (**4**).* Reduction of 1-(3-(nitromethyl)oxetan-3-yl)pyrrolidine (**3**) was performed as described in McLaughlin *et al.*[10] to a stirred solution of SM (**3**) (1 eq) in THF and followed by the addition of Raney nickel. The reaction mixture was stirred for 3 h under a hydrogen balloon. After completion of the reaction, the reaction mixture was filtered through a Celite bed. The solvent was evaporated under a vacuum, and the crude product was purified by column chromatography (MeOH:DCM, 1:9 → 2:8) to give compound (**4**) as a liquid.

https://doi.org/10.1021/acs.jmedchem.1c02075
J. Med. Chem. 2022, 65, 10920−10937

General Procedure for the Synthesis of General Compound (5) (FTO-1-53 N). A two-necked round-bottom flask was charged with compound (**4**) (1 eq) in MeOH and followed by the addition of corresponding aldehyde (1 eq). The reaction mixture was stirred for 3 h at room temperature. After the starting materials had been consumed, the reaction mixture was slowly treated with $NaBH_4$ (1.5 eq). The reaction mass was again stirred for 2 h at room temperature. After completion of the reaction, the crude product was concentrated under vacuum, dissolved in water, and extracted with ethyl acetate (3 × 15 mL). The organic layers were combined, dried with $NaSO_4$, and filtered. The filtrate was concentrated under vacuum to afford the crude product. The crude material was purified by flash column chromatography (MeOH:DCM, 1:9 → 2:8) to give the final compound (**5**) as an oil.

Compound Characterization. The Supporting Information provides a detailed description of the solvent purification and general methods for the synthesis and purification of each analogue. All compounds were purified by column chromatography and characterized by ^{1}H and ^{13}C NMR and HRMS. Purity was determined by HPLC at >95% for all compounds. Spectra can be found in the Supporting Information.

1-(3-(Pyrrolidin-1-yl)oxetan-3-yl)-N,N-bis(3-(trifluoromethyl)-benzyl)methanamine (FTO-01 N). ^{1}H NMR (600 MHz, $CDCl_3$): δ 7.60 (s, 2H), 7.48 (t, J = 6.3 Hz, 4H), 7.41 (t, J = 7.7 Hz, 2H), 4.75 (d, J = 6.8 Hz, 2H), 4.36 (d, J = 6.6 Hz, 2H), 3.63 (s, 4H), 2.87 (s, 4H), 2.76 (s, 2H), 2.76 (*d*, J = 12.1 Hz, 2 H), 1.80 (dd, J = 10.2, 3.0 Hz, 2H). ^{13}C NMR (151 MHz, $CDCl_3$): δ 140.8, 140.8, 131.0, 131.0, 130.7 (q, CF_3), 130.7 (q, CF_3), 127.0, 127.0, 125.8, 125.8, 125.2, 123.4, 123.4, 121.6, 77.5, 77.5, 63.3, 59.1, 58.6, 58.6, 46.7, 46.7, 24.0, 24.0. HRMS (ESI): m/z calculated for $C_{24}H_{26}F_6N_2O$ 472.1949, found 473.2016 (M + H$^+$). Purity > 98%.

1-(3-(Pyrrolidin-1-yl)oxetan-3-yl)-N-(3-(trifluoromethyl)benzyl)-methanamine (FTO-02 N). ^{1}H NMR (600 MHz, $CDCl_3$): δ 7.60 (s, 1H), 7.55−7.49 (m, 2H), 7.44 (t, J = 7.7 Hz, 1H), 4.79 (d, J = 6.6 Hz, 2H), 4.34 (d, J = 6.7 Hz, 2H), 3.89 (s, 2H), 2.95 (s, 2H), 2.88 (s, 1H), 2.76−2.67 (m, 4H), 1.84−1.75 (m, 4H). ^{13}C NMR (151 MHz, $CDCl_3$): δ 141.7, 131.6, 130.9 (q, CF_3), 128.9, 124.9, 124.0, 123.5, 77.5, 77.5, 62.7, 54.7, 53.6, 46.7, 46.7, 24.0, 24.0. HRMS (ESI): m/z calculated for $C_{16}H_{21}F_3N_2O$ 314.1606, found 315.1677 (M + H$^+$). Purity > 96%.

1-(3-(Pyrrolidin-1-yl)oxetan-3-yl)-N-(4-(trifluoromethyl)benzyl)-methanamine (FTO-03 N). ^{1}H NMR (600 MHz, $CDCl_3$): δ 7.57 (d, J = 8.0 Hz, 2H), 7.45 (d, J = 7.9 Hz, 2H), 4.78 (d, J = 6.6 Hz, 2H), 4.34 (d, J = 6.6 Hz, 2H), 3.89 (s, 2H), 2.95 (s, 2H), 2.73−2.68 (m, 4H), 1.83−1.76 (m, 4H). ^{13}C NMR (151 MHz, $CDCl_3$): δ 144.8, 129.4 (q, CF_3), 128.4, 128.4, 125.4, 125.4, 123.5, 77.0, 77.0, 62.7, 54.70, 53.6, 46.9, 46.9, 24.1, 24.1. HRMS (ESI): m/z calculated for $C_{16}H_{21}F_3N_2O$ 314.1606, found 315.1679 (M + H$^+$). Purity > 98%.

1-(3-(Pyrrolidin-1-yl)oxetan-3-yl)-N-(4-(trifluoromethoxy)-benzyl)methanamine (FTO-04 N). ^{1}H NMR (600 MHz, $CDCl_3$): δ 7.36 (d, J = 8.7 Hz, 2H), 7.17 (d, J = 8.4 Hz, 2H), 4.79 (d, J = 6.6 Hz, 2H), 4.35 (d, J = 6.6 Hz, 2H), 3.83 (s, 2H), 2.94 (s, 2H), 2.72−2.67 (m, 4H), 1.84−1.77 (m, 4H). ^{13}C NMR (151 MHz, $CDCl_3$): δ 148.3, 139.4, 129.5, 129.5, 121.5, 121.1, 121.1, 77.0, 77.0, 62.7, 54.7, 53.3, 46.9, 46.9, 24.1, 24.1. HRMS (ESI): m/z calculated for $C_{16}H_{21}F_3N_2O_2$ 330.1555, found 331.1627 (M + H$^+$). Purity > 95%.

N-(4-Nitrobenzyl)-1-(3-(pyrrolidin-1-yl)oxetan-3-yl)-methanamine (FTO-05 N). ^{1}H NMR (600 MHz, $CDCl_3$): δ 8.19 (d, J = 8.7 Hz, 2H), 7.52 (d, J = 8.7 Hz, 2H), 4.80 (d, J = 6.6 Hz, 2H), 4.34 (d, J = 6.7 Hz, 2H), 3.94 (s, 2H), 2.95 (s, 2H), 2.75−2.68 (m, 4H), 1.84−1.77 (m, 4H). ^{13}C NMR (151 MHz, $CDCl_3$): δ 148.5, 147.2, 128.8, 128.8, 123.8, 123.8, 76.9, 76.9, 62.7, 54.9, 53.4, 47.0, 47.0, 24.1, 24.1. HRMS (ESI): m/z calculated for $C_{15}H_{21}N_3O_3$ 291.1583, found 292.1656 (M + H$^+$). Purity > 96%.

N-(4-(tert-Butyl)benzyl)-1-(3-(pyrrolidin-1-yl)oxetan-3-yl)-methanamine (FTO-06 N). ^{1}H NMR (600 MHz, $CDCl_3$): δ 7.35 (d, J = 8.3 Hz, 2H), 7.26 (d, J = 8.7 Hz, 2H), 5.29 (s, 1H), 4.77 (d, J = 6.6 Hz, 2H), 4.37 (d, J = 6.6 Hz, 2H), 3.82 (s, 2H), 2.96 (m, 2H), 2.68 (t, J = 6.4 Hz, 4H), 1.82−1.77 (m, 4H), 1.31 (s, 9H). ^{13}C NMR (151 MHz, $CDCl_3$): δ 150.1, 137.2, 128.0, 128.0, 125.4, 125.4, 77.0, 77.0, 62.6, 54.5, 53.6, 46.9, 46.9, 34.6, 31.5, 31.5, 31.5, 24.1, 24.1. HRMS (ESI): m/z calculated for $C_{19}H_{30}N_2O$ 302.2358, found 303.2428 (M + H$^+$). Purity > 96%.

N-(4-Bromobenzyl)-1-(3-(pyrrolidin-1-yl)oxetan-3-yl)-methanamine (FTO-07 N). ^{1}H NMR (600 MHz, $CDCl_3$): δ 7.44 (d, J = 8.3 Hz, 2H), 7.21 (d, J = 8.3 Hz, 2H), 4.78 (d, J = 6.6 Hz, 2H), 4.33 (d, J = 6.6 Hz, 2H), 3.78 (s, 2H), 2.92 (s, 2H), 2.69 (t, J = 6.5 Hz, 4H), 1.83−1.77 (m, 4H). ^{13}C NMR (151 MHz, $CDCl_3$): δ 139.6, 131.5, 131.5, 129.9, 129.9, 120.8, 77.0, 77.0, 62.6, 54.6, 53.4, 47.0, 47.0, 24.1, 24.1. HRMS (ESI): m/z calculated for $C_{15}H_{21}BrN_2O$ 324.0837, found 325.0907 (M + H$^+$). Purity > 98%.

1-(Pyridin-2-yl)-N-((3-(pyrrolidin-1-yl)oxetan-3-yl)methyl)-methanamine (FTO-08 N). ^{1}H NMR (600 MHz, $CDCl_3$): δ 8.54 (d, J = 4.6 Hz, 1H), 7.64 (td, J = 7.6, 1.8 Hz, 1H), 7.35 (d, J = 7.8 Hz, 1H), 7.15 (ddd, J = 7.6, 4.9, 1.2 Hz, 1H), 4.79 (d, J = 6.6 Hz, 2H), 4.37 (d, J = 6.6 Hz, 2H), 3.96 (s, 2H), 3.00 (s, 2H), 2.72 (m, 4H), 2.49 (broad s, 1 H), 1.84−1.75 (m, 4H). ^{13}C NMR (151 MHz, $CDCl_3$): δ 160.1, 149.4, 136.6, 122.4, 122.1, 77.0, 77.0, 62.7, 55.4, 54.9, 46.9, 46.9, 24.1, 24.1. HRMS (ESI): m/z calculated for $C_{14}H_{21}N_3O$ 247.1685, found 248.1759 (M + H$^+$). Purity >99%.

1-(5-Methyl-1H-indol-3-yl)-N-((3-(pyrrolidin-1-yl)oxetan-3-yl)-methyl)methanamine (FTO-09 N). ^{1}H NMR (600 MHz, $CDCl_3$): δ 8.28 (s, 1H), 7.43 (s, 1H), 7.26 (d, J = 8.2 Hz, 1H), 7.16 (d, J = 2.4 Hz, 1H), 7.03 (dd, J = 8.3, 1.6 Hz, 1H), 4.77 (d, J = 6.7 Hz, 2H), 4.39 (d, J = 6.7 Hz, 2H), 4.07 (s, 2H), 3.08 (s, 2H), 2.61 (t, J = 6.1 Hz, 4H), 2.45 (s, 3H), 1.73−1.69 (m, 4H). ^{13}C NMR (151 MHz, $CDCl_3$): δ 134.8, 129.1, 127.4, 124.0, 123.5, 118.4, 116.4, 111.1, 76.9, 76.9, 62.3, 55.9, 53.9, 46.8, 44.7, 23.9, 23.9, 21.7. HRMS (ESI): m/z calculated for $C_{18}H_{25}N_3O$ 299.1998, found 300.2070 (M + H$^+$). Purity > 98%.

1-(Pyridin-3-yl)-N-((3-(pyrrolidin-1-yl)oxetan-3-yl)methyl)-methanamine (FTO-10 N). ^{1}H NMR (600 MHz, $CDCl_3$): δ 8.56 (d, J = 2.5 Hz, 1H), 8.50 (dd, J = 4.8, 1.7 Hz, 1H), 7.69 (dt, J = 7.8, 2.0 Hz, 1H), 7.28 (q, J = 4.7 Hz, 1H), 4.78 (d, J = 6.6 Hz, 2H), 4.33 (d, J = 6.6 Hz, 2H), 3.85 (s, 2H), 2.95 (s, 2H), 2.70 (t, J = 6.2 Hz, 4H), 1.82−1.77 (m, 4H). ^{13}C NMR (151 MHz, $CDCl_3$): δ 149.9, 148.7, 135.9, 135.9, 123.5, 76.9, 76.9, 62.7, 54.7, 51.4, 46.9, 46.9, 24.1, 24.1. HRMS (ESI): m/z calculated for $C_{14}H_{21}N_3O$ 247.1685, found 248.1759 (M + H$^+$). Purity > 95%.

1-(5-Fluoro-1H-indol-3-yl)-N-((3-(pyrrolidin-1-yl)oxetan-3-yl)-methyl)methanamine (FTO-11 N). ^{1}H NMR (600 MHz, $CDCl_3$): δ 8.40 (s, 1H), 7.32−7.27 (m, 2H), 7.26 (dq, J = 2.8, 0.9 Hz, 1H), 6.95 (td, J = 9.0, 2.5 Hz, 1H), 4.78 (d, J = 6.7 Hz, 2H), 4.38 (d, J = 6.7 Hz, 2H), 4.04 (s, 2H), 3.07 (s, 2H), 2.65 (q, J = 4.5 Hz, 4H), 1.77−1.72 (m, 4H). ^{13}C NMR (151 MHz, $CDCl_3$): δ 158.7, 157.2, 133.0, 127.6, 127.6, 112.1, 110.8, 103.9, 77.2, 77.2, 62.4, 54.1, 51.0, 46.9, 44.7, 24.0, 24.0. HRMS (ESI): m/z calculated for $C_{17}H_{22}FN_3O$ 303.1747, found 304.1819 (M + H$^+$). Purity > 97%.

1-(6-Fluoro-1H-indol-3-yl)-N-((3-(pyrrolidin-1-yl)oxetan-3-yl)-methyl)methanamine (FTO-12 N). ^{1}H NMR (600 MHz, $CDCl_3$): δ 8.44 (s, 1H), 7.57 (dd, J = 8.7, 5.2 Hz, 1H), 7.21 (d, J = 2.8 Hz, 1H), 7.06 (dd, J = 9.6, 2.3 Hz, 1H), 6.89 (ddd, J = 9.6, 8.7, 2.3 Hz, 1H), 4.77 (d, J = 6.7 Hz, 2H), 4.37 (d, J = 6.8 Hz, 2H), 4.09 (s, 2H), 3.08 (s, 2H), 2.62 (q, J = 4.9 Hz, 4H), 1.76−1.68 (m, 4H). ^{13}C NMR (151 MHz, $CDCl_3$): δ 161.0, 159.4, 136.5, 136.4, 123.7, 119.6, 108.7, 97.7, 76.8, 76.8, 62.4, 53.8, 50.4, 46.9, 46.9, 24.0, 24.0. HRMS (ESI): m/z calculated for $C_{17}H_{22}FN_3O$, 303.1747 found 304.1819 (M + H$^+$). Purity > 97%.

N-((1H-Indol-3-yl)methyl)-1-(3-(pyrrolidin-1-yl)oxetan-3-yl)-methanamine (FTO-13 N). ^{1}H NMR (600 MHz, $CDCl_3$): δ 8.35 (s, 1H), 7.65 (dd, J = 7.9, 1.1 Hz, 1H), 7.39 (d, J = 8.2 Hz, 1H), 7.27 (d, J = 4.5 Hz, 1H), 7.21 (ddd, J = 8.1, 7.0, 1.2 Hz, 1H), 7.14 (ddd, J = 8.0, 7.0, 1.1 Hz, 1H), 4.76 (d, J = 6.8 Hz, 2H), 4.39 (d, J = 6.8 Hz, 2H), 4.14 (s, 2H), 3.11 (s, 2H), 2.61 (t, J = 6.4 Hz, 4H), 1.75−1.66 (m, 4H). ^{13}C NMR (151 MHz, $CDCl_3$): δ 136.5, 127.1, 123.5, 122.5, 122.0, 119.9, 118.6, 111.5, 76.7, 76.7, 62.3, 50.4, 46.9, 46.9, 44.5, 23.9, 23.9. HRMS (ESI): m/z calculated for $C_{17}H_{23}N_3O$, 285.1841 found 286.1916 (M + H$^+$). Purity > 95%.

1-(7-Methoxy-1H-indol-3-yl)-N-((3-(pyrrolidin-1-yl)oxetan-3-yl)-methyl)methanamine (FTO-14 N). ^{1}H NMR (600 MHz, $CDCl_3$): δ 8.37 (s, 1H), 7.25 (d, J = 8.0 Hz, 1H), 7.23 (broad s, 1H), 7.06 (t, J =

https://doi.org/10.1021/acs.jmedchem.1c02075
J. Med. Chem. 2022, 65, 10920−10937

7.8 Hz, 1H), 6.66 (d, J = 7.7 Hz, 1H), 4.76 (d, J = 6.7 Hz, 2H), 4.39 (d, J = 6.7 Hz, 2H), 4.11 (s, 2H), 3.96 (s, 3H), 3.09 (s, 2H), 2.61 (t, J = 5.8 Hz, 4H), 1.74−1.66 (m, 4H). ^{13}C NMR (151 MHz, $CDCl_3$): δ 146.4, 128.5, 127.0, 123.7, 120.4, 114.0, 111.4, 102.2, 76.7, 76.7, 62.2, 55.7, 55.5, 53.4, 46.8, 46.8, 23.9, 23.9. HRMS (ESI): m/z calculated for $C_{18}H_{25}N_3O_2$ 315.1947, found 316.2018 (M + H$^+$). Purity > 95%.

1-(6-Methoxy-1H-indol-3-yl)-N-((3-(pyrrolidin-1-yl)oxetan-3-yl)-methyl)methanamine (FTO-15 N). ^{1}H NMR (600 MHz, $CDCl_3$): δ 8.19 (s, 1H), 7.51 (d, J = 8.6 Hz, 1H), 7.13 (d, J = 2.3 Hz, 1H), 6.87 (d, J = 2.2 Hz, 1H), 6.80 (dd, J = 8.7, 2.2 Hz, 1H), 4.75 (d, J = 6.8 Hz, 2H), 4.38 (d, J = 6.7 Hz, 2H), 4.09 (s, 2H), 3.84 (s, 3H), 3.09 (s, 2H), 2.59 (q, J = 4.4 Hz, 4H), 1.72−1.68 (m, 4H). ^{13}C NMR (151 MHz, $CDCl_3$): δ 156.8, 137.3, 122.3, 121.5, 119.3, 119.3, 109.9, 94.9, 76.7, 76.7, 62.2, 55.8, 51.0, 46.8, 46.8, 44.5, 23.9, 23.9. HRMS (ESI): m/z calculated for $C_{18}H_{25}N_3O_2$ 315.1947, found 316.2018 (M + H$^+$). Purity > 99%.

1-(7-Fluoro-1H-indol-3-yl)-N-((3-(pyrrolidin-1-yl)oxetan-3-yl)-methyl)methanamine (FTO-16 N). ^{1}H NMR (600 MHz, $CDCl_3$): δ 8.49 (s, 1H), 7.42 (d, J = 7.9 Hz, 1H), 7.24 (s, 1H), 7.04 (td, J = 7.9, 2.0 Hz, 1H), 6.98−6.94 (m, 1H), 6.93−6.89 (m, 1H), 4.77 (d, J = 6.8 Hz, 2H), 4.38 (d, J = 6.7 Hz, 2H), 4.10 (s, 2H), 3.08 (s, 2H), 2.62 (t, J = 5.9 Hz, 4H), 1.74−1.69 (m, 4H). ^{13}C NMR (151 MHz, $CDCl_3$): δ 150.6, 148.9, 130.9, 124.9, 120.1, 117.6, 114.6, 107.3, 76.8, 76.8, 62.4, 53.9, 46.9, 46.9, 44.6, 24.0, 24.0. HRMS (ESI): m/z calculated for $C_{17}H_{23}FN_3O$ 303.1747, found 304.1820 (M + H$^+$). Purity > 95%.

1-(4-Fluoro-1H-indol-3-yl)-N-((3-(pyrrolidin-1-yl)oxetan-3-yl)-methyl)methanamine (FTO-17 N). ^{1}H NMR (600 MHz, $CDCl_3$): δ 8.57 (s, 1H), 7.18−7.09 (m, 3H), 7.09 (td, J = 8.0, 5.1 Hz, 1H), 6.77 (dd, J = 7.8, 3.1 Hz, 1H), 4.78 (d, J = 6.7 Hz, 2H), 4.40 (d, J = 6.7 Hz, 2H), 4.12 (s, 2H), 3.11 (s, 2H), 2.61 (t, J = 6.0 Hz, 4H), 1.77−1.68 (m, 4H). ^{13}C NMR (151 MHz, $CDCl_3$): δ 157.9, 156.3, 139.3, 122.9, 122.9, 115.7, 107.7, 104.8, 76.9, 76.9, 62.3, 53.9, 46.8, 46.8, 45.5, 23.9, 23.9. HRMS (ESI): m/z calculated for $C_{17}H_{23}FN_3O$ 303.1747, found 304.1820 (M + H$^+$). Purity > 97%.

1-(4-Methyl-1H-indol-3-yl)-N-((3-(pyrrolidin-1-yl)oxetan-3-yl)-methyl)methanamine (FTO-18 N). ^{1}H NMR (600 MHz, $CDCl_3$): δ 8.12 (s, 1H), 7.54 (d, J = 8.1 Hz, 1H), 7.20 (d, J = 2.5 Hz, 1H), 7.08 (t, J = 7.6 Hz, 1H), 7.01 (d, J = 7.3 Hz, 1H), 4.75 (d, J = 6.7 Hz, 2H), 4.39 (d, J = 6.7 Hz, 2H), 4.08 (s, 2H), 3.08 (s, 2H), 2.66 (t, J = 5.9 Hz, 4H), 2.50 (s, 3H), 1.79−1.66 (m, 4H).^{13}C NMR (151 MHz, $CDCl_3$): δ 137.1, 130.8, 125.0, 123.7, 122.2, 121.1, 115.1, 109.2, 77.0, 77.0, 62.6, 54.6, 46.8, 46.8, 46.5, 24.0, 24.0, 20.1. HRMS (ESI): m/z calculated for $C_{18}H_{25}N_3O$ 299.1998, found 304.1820 (M + H$^+$). Purity > 96%.

1-(3-(Pyrrolidin-1-yl)oxetan-3-yl)-N-(2-(trifluoromethyl)benzyl)-methanamine (FTO-19 N). ^{1}H NMR (600 MHz, $CDCl_3$): δ 7.67 (d, J = 7.7 Hz, 1H), 7.63 (d, J = 7.8 Hz, 1H), 7.53 (t, J = 7.6 Hz, 1H), 7.34 (t, J = 7.6 Hz, 1H), 4.80 (d, J = 6.6 Hz, 2H), 4.37 (d, J = 6.6 Hz, 2H), 3.99 (s, 2H), 2.99 (s, 2H), 2.70 (t, J = 6.3 Hz, 4H), 1.82−1.74 (m, 4H). ^{13}C NMR (151 MHz, $CDCl_3$): δ 139.2, 132.0, 130.4, 128.4 (q, CF_3), 125.9, 125.6, 123.8, 77.0, 77.0, 62.6, 54.9, 50.0, 46.8, 46.8, 24.1, 24.1. HRMS (ESI): m/z calculated for $C_{16}H_{21}F_3N_2O$ 314.1606, found 315.1678 (M + H$^+$). Purity > 95%.

N-(3-Methoxybenzyl)-1-(3-(pyrrolidin-1-yl)oxetan-3-yl)-methanamine (FTO-20 N). ^{1}H NMR (600 MHz, $CDCl_3$): δ 7.24 (t, J = 7.8 Hz, 1H), 6.91 (d, J = 6.0 Hz, 2H), 6.80 (dd, J = 7.5, 1.9 Hz, 1H), 4.78 (d, J = 6.6 Hz, 2H), 4.36 (d, J = 6.6 Hz, 2H), 3.82 (d, J = 7.5 Hz, 2H), 3.83 (s, 3H), 2.95 (s, 2H), 2.69 (t, J = 6.3 Hz, 4H), 1.84−1.75 (m, 4H). ^{13}C NMR (151 MHz, $CDCl_3$): δ 159.8, 141.9, 129.6, 120.5, 113.7, 112.6, 76.9, 76.9, 62.6, 55.3, 54.3, 53.8, 46.8, 46.8, 24.0, 24.0. HRMS (ESI): m/z calculated for $C_{16}H_{24}N_2O_2$ 276.1838, found 277.1911 (M + H$^+$). Purity > 95%.

N-(2-Methoxybenzyl)-1-(3-(pyrrolidin-1-yl)oxetan-3-yl)-methanamine (FTO-21 N). ^{1}H NMR (600 MHz, $CDCl_3$): δ 7.29−7.22 (m, 2H), 6.93 (t, J = 7.4 Hz, 1H), 6.87 (d, J = 8.4 Hz, 1H), 4.76 (d, J = 6.7 Hz, 2H), 4.39 (d, J = 6.7 Hz, 2H), 3.88 (s, 2H), 3.83 (s, 3H), 2.97 (s, 2H), 2.60 (t, J = 6.2 Hz, 4H), 1.79−1.72 (m, 4H). ^{13}C NMR (151 MHz, $CDCl_3$): δ 157.8, 130.5, 128.9, 126.9, 120.6, 110.2, 76.8, 76.8, 62.3, 55.2, 53.8, 49.5, 46.6, 46.6, 24.0, 24.0. HRMS (ESI): m/z calculated for $C_{16}H_{24}N_2O_2$ 276.1838, found 277.1911 (M + H$^+$). Purity > 95%.

N-(2,4-Bis(trifluoromethyl)benzyl)-1-(3-(pyrrolidin-1-yl)oxetan-3-yl)methanamine (FTO-22 N). ^{1}H NMR (600 MHz, $CDCl_3$): δ 7.92 (d, J = 8.2 Hz, 1H), 7.88 (s, 1H), 7.80 (dd, J = 8.1, 1.9 Hz, 1H), 4.81 (d, J = 6.6 Hz, 2H), 4.36 (d, J = 6.6 Hz, 2H), 4.05 (s, 2H), 3.00 (s, 2H), 2.72 (t, J = 5.8 Hz, 4H), 1.85−1.76 (m, 4H). ^{13}C NMR (151 MHz, $CDCl_3$): δ 143.8, 136.4, 130.8, 129.6, 129.4, 128.8, 124.8, 123.0 76.6, 76.6, 62.7, 55.1, 49.6, 47.0, 47.0, 24.1, 24.1. HRMS (ESI): m/z calculated for $C_{17}H_{20}F_6N_2O$ 382.1480, found 383.1554 (M + H$^+$). Purity > 95%.

N-(3,5-Dimethoxybenzyl)-1-(3-(pyrrolidin-1-yl)oxetan-3-yl)-methanamine (FTO-23 N). ^{1}H NMR (600 MHz, $CDCl_3$): δ 6.50 (d, J = 2.3 Hz, 2H), 6.35 (t, J = 2.3 Hz, 1H), 4.78 (d, J = 6.7 Hz, 2H), 4.36 (d, J = 6.6 Hz, 2H), 3.79 (s, 8H), 2.95 (s, 2H), 2.70 (t, J = 6.2 Hz, 4H), 1.81−1.77 (m, 4H). ^{13}C NMR (151 MHz, $CDCl_3$): δ 161.0, 161.0, 142.8, 106.0, 106.0, 99.1, 77.0, 77.0, 62.6, 55.4, 55.4, 54.3, 54.0, 46.9, 46.9, 24.1, 24.1. HRMS (ESI): m/z calculated for $C_{17}H_{26}N_2O_3$ 306.1943, found 307.2016 (M + H$^+$). Purity > 95%.

N-(4-Ethoxybenzyl)-1-(3-(pyrrolidin-1-yl)oxetan-3-yl)-methanamine (FTO-24 N). ^{1}H NMR (600 MHz, $CDCl_3$): δ 7.23 (d, J = 8.5 Hz, 2H), 6.86 (d, J = 8.6 Hz, 2H), 4.77 (d, J = 6.6 Hz, 2H), 4.35 (d, J = 6.6 Hz, 2H), 4.02 (q, J = 7.0 Hz, 2H), 3.79 (s, 2H), 2.94 (s, 2H), 2.67 (t, J = 6.1 Hz, 4H), 1.80−1.76 (m, 4H), 1.41 (t, J = 7.0 Hz, 3H). ^{13}C NMR (151 MHz, $CDCl_3$): δ 158.2, 132.0, 129.5, 129.5, 114.5, 114.5, 77.0, 77.0, 63.5, 62.6, 63.6, 54.1, 53.3, 46.8, 46.8, 24.1, 24.1. HRMS (ESI): m/z calculated for $C_{17}H_{26}N_2O_2$ 290.1994, found 291.2068 (M + H$^+$). Purity > 95%.

N-(2,5-Dimethylbenzyl)-1-(3-(pyrrolidin-1-yl)oxetan-3-yl)-methanamine (FTO-25 N). ^{1}H NMR (600 MHz, $CDCl_3$): δ 7.10 (s, 1H), 7.04 (d, J = 7.6 Hz, 1H), 6.97 (d, J = 7.5 Hz, 1H), 4.79 (d, J = 6.6 Hz, 2H), 4.38 (d, J = 6.6 Hz, 2H), 3.78 (s, 2H), 3.00 (s, 2H), 2.68 (t, J = 6.1 Hz, 4H), 2.31 (d, J = 5.1 Hz, 6H), 1.80−1.76 (m, 4H). ^{13}C NMR (151 MHz, $CDCl_3$): δ 137.9, 135.3, 133.3, 130.3, 129.6, 127.8, 77.0, 77.0, 62.6, 54.8, 51.9, 46.8, 46.8, 24.0, 24.0, 21.1, 18.6. HRMS (ESI): m/z calculated for $C_{17}H_{26}N_2O$ 275.2045, found 275.2119 (M + H$^+$). Purity > 95%.

(4-(((((3-(Pyrrolidin-1-yl)oxetan-3-yl)methyl)amino)methyl)-phenyl)methanol (FTO-26 N). ^{1}H NMR (600 MHz, $CDCl_3$): δ 8.00 (d, J = 8.3 Hz, 2H), 7.40 (d, J = 8.1 Hz, 2H), 4.78 (d, J = 6.6 Hz, 2H), 4.34 (d, J = 6.6 Hz, 2H), 3.90 (s, 3H), 3.89 (s, 2H), 2.93 (s, 2H), 2.69 (t, J = 6.2 Hz, 4H), 1.90 (broad s, 1H), 1.81−1.77 (m, 4H). ^{13}C NMR (151 MHz, $CDCl_3$): δ 167.1, 146.0, 129.8, 129.8, 128.1, 128.1, 76.9, 76.9, 62.7, 54.6, 53.7, 52.2, 46.9, 46.9, 24.1, 24.1. HRMS (ESI): m/z calculated for $C_{16}H_{24}N_2O_2$ 276.1838, found 277.1918 (M + H$^+$). Purity > 95%.

1-(2,3-Dihydrobenzo[b][1,4]dioxin-6-yl)-N-((3-(pyrrolidin-1-yl)-oxetan-3-yl)methyl)methanamine (FTO-27 N). ^{1}H NMR (600 MHz, $CDCl_3$): δ 6.85 (d, J = 1.8 Hz, 1H), 6.83−6.77 (m, 2H), 4.77 (d, J = 6.7 Hz, 2H), 4.36 (d, J = 6.6 Hz, 2H), 4.25 (s, 4H), 3.74 (s, 2H), 2.95 (s, 2H), 2.69 (t, J = 6.1 Hz, 4H), 1.81−1.77 (m, 4H). ^{13}C NMR (151 MHz, $CDCl_3$): δ 143.5, 142.6, 133.8, 121.2, 117.2, 117.0, 77.0, 77.0, 64.5, 64.5, 62.6, 54.3, 53.4, 46.9, 46.9, 24.1, 24.1. HRMS (ESI): m/z calculated for $C_{17}H_{24}N_2O_3$ 304.1787, found 305.1859 (M + H$^+$). Purity > 98%.

N-(3,5-Dimethoxybenzyl)-1-(3-(pyrrolidin-1-yl)oxetan-3-yl)-methanamine (FTO-28 N). ^{1}H NMR (600 MHz, $CDCl_3$): δ 6.51 (d, J = 2.3 Hz, 2H), 6.35 (t, J = 2.3 Hz, 1H), 4.78 (d, J = 6.6 Hz, 2H), 4.36 (d, J = 6.6 Hz, 2H), 3.79 (s, 8H), 2.95 (s, 2H), 2.70 (t, J = 6.2 Hz, 4H), 1.81−1.78 (m, 4H). ^{13}C NMR (151 MHz, $CDCl_3$): δ 161.0, 161.0, 142.8, 106.1, 106.1, 99.1, 77.0, 77.0, 62.6, 55.5, 55.5, 54.3, 54.0, 46.9, 46.9, 24.1, 24.1. HRMS (ESI): m/z calculated for $C_{17}H_{26}N_2O_3$ 306.1943, found 307.2017 (M + H$^+$). Purity > 95%.

N-(3,4-Dimethoxybenzyl)-1-(3-(pyrrolidin-1-yl)oxetan-3-yl)-methanamine (FTO-29 N). ^{1}H NMR (600 MHz, $CDCl_3$): δ 6.91 (d, J = 1.9 Hz, 1H), 6.87−6.78 (m, 2H), 4.79 (broad s, 1H), 4.77 (d, J = 6.6 Hz, 2H), 4.35 (d, J = 6.7 Hz, 2H), 3.87 (d, J = 7.5 Hz, 6H), 3.79 (s, 2H), 2.94 (s, 2H), 2.68 (t, J = 6.1 Hz, 4H), 1.81−1.76 (m, 4H). ^{13}C NMR (151 MHz, $CDCl_3$): δ 149.1, 148.2, 132.4, 120.5, 111.3, 111.0, 76.9, 76.9, 62.5, 56.0, 56.0, 54.0, 53.6, 46.8, 46.8, 24.1, 24.1.

https://doi.org/10.1021/acs.jmedchem.1c02075
J. Med. Chem. 2022, 65, 10920−10937

HRMS (ESI): *m/z* calculated for $C_{17}H_{26}N_2O_3$ 306.1943, found 307.2018 (M + H^+). Purity > 95%.

N-(3,4-Dimethylbenzyl)-1-(3-(pyrrolidin-1-yl)oxetan-3-yl)-methanamine (FTO-30 N). ^{1}H NMR (600 MHz, $CDCl_3$): δ 7.10 (s, 1H), 7.09 (d, *J* = 8.3 Hz, 1H), 7.06 (d, *J* = 7.1 Hz, 1H), 4.78 (d, *J* = 6.6 Hz, 2H), 4.36 (d, *J* = 6.6 Hz, 2H), 3.79 (s, 2H), 2.95 (s, 2H), 2.68 (q, *J* = 5.0 Hz, 4H), 2.25 (d, *J* = 7.3 Hz, 6H), 1.82−1.76 (m, 4H). ^{13}C NMR (151 MHz, $CDCl_3$): δ 137.2, 136.7, 135.5, 129.8, 129.7, 125.7, 76.9, 76.9, 62.5, 54.1, 53.5, 46.8, 46.8, 24.1, 24.1, 19.9, 19.6. HRMS (ESI): *m/z* calculated for $C_{17}H_{26}N_2O$ 274.2045, found 275.2121 (M + H^+). Purity > 98%.

1-(8-Methylquinolin-3-yl)-N-((3-(pyrrolidin-1-yl)oxetan-3-yl)-methyl)methanamine (FTO-31 N). ^{1}H NMR (600 MHz, $CDCl_3$): δ 8.93 (d, *J* = 2.1 Hz, 1H), 8.07 (d, *J* = 2.2 Hz, 1H), 7.65 (d, *J* = 8.1 Hz, 1H), 7.54 (d, *J* = 7.0 Hz, 1H), 7.43 (t, *J* = 7.5 Hz, 1H), 4.78 (d, *J* = 6.6 Hz, 2H), 4.36 (d, *J* = 6.6 Hz, 2H), 4.04 (s, 2H), 3.01 (s, 2H), 2.82 (s, 3H), 2.72 (t, *J* = 6.5 Hz, 4H), 1.83−1.77 (m, 4H). ^{13}C NMR (151 MHz, $CDCl_3$): δ 150.5, 146.8, 137.1, 135.1, 132.8, 129.4, 128.1, 126.3, 124.9, 77.0, 77.0, 62.6, 57.1, 51.7, 51.7, 47.1, 24.1, 24.1, 18.1. HRMS (ESI): *m/z* calculated for $C_{19}H_{25}N_3O$ 311.1998, found 312.2072 (M + H^+). Purity > 99%.

2,6-Dimethoxy-4-(((((3-(pyrrolidin-1-yl)oxetan-3-yl)methyl)-amino)methyl)phenol (FTO-32 N). ^{1}H NMR (600 MHz, $CDCl_3$): δ 6.62 (s, 2H), 4.78 (d, *J* = 6.8 Hz, 2H), 4.38 (d, *J* = 6.7 Hz, 2H), 3.89 (s, 6H), 3.82 (s, 2H), 2.97 (s, 2H), 2.70 (t, *J* = 5.4 Hz, 4H), 1.82−1.77 (m, 4H). ^{13}C NMR (151 MHz, $CDCl_3$): δ 147.2, 147.2, 134.0, 105.3, 105.1, 105.1, 76.8, 76.8, 62.5, 56.4, 56.4, 53.8, 53.3, 46.9, 46.9, 24.1, 24.1. HRMS (ESI): *m/z* calculated for $C_{17}H_{26}N_2O_4$ 322.1893, found 323.1966 (M + H^+). Purity > 97%.

1-(6-Methylpyridin-3-yl)-N-((3-(pyrrolidin-1-yl)oxetan-3-yl)-methyl)methanamine (FTO-33 N). ^{1}H NMR (600 MHz, $CDCl_3$): δ 8.42 (d, *J* = 2.3 Hz, 1H), 7.58 (dd, *J* = 7.9, 2.3 Hz, 1H), 7.12 (d, *J* = 7.9 Hz, 1H), 4.77 (d, *J* = 6.6 Hz, 2H), 4.33 (d, *J* = 6.6 Hz, 2H), 3.80 (s, 2H), 2.93 (s, 2H), 2.73 (t, *J* = 5.8 Hz, 4H), 2.54 (s, 3H), 1.82−1.77 (m, 4H). ^{13}C NMR (151 MHz, $CDCl_3$): δ 157.2, 149.0, 136.5, 132.6, 123.2, 76.9, 76.9, 62.7, 54.4, 51.1, 46.9, 46.9, 24.2, 24.1, 24.1. HRMS (ESI): *m/z* calculated for $C_{15}H_{23}N_3O$ 261.1841, found 262.1917 (M + H^+). Purity > 95%.

N,N-Dimethyl-4-((((3-(pyrrolidin-1-yl)oxetan-3-yl)methyl)-amino)methyl)aniline (FTO-34 N). ^{1}H NMR (600 MHz, $CDCl_3$): δ 7.23 (d, *J* = 8.6 Hz, 2H), 6.71 (d, *J* = 8.6 Hz, 2H), 4.77 (d, *J* = 6.8 Hz, 2H), 4.38 (d, *J* = 6.8 Hz, 2H), 3.85 (s, 2H), 3.02 (s, 2H), 2.94 (s, 6H), 2.65 (t, *J* = 6.0 Hz, 4H), 1.79−1.75 (m, 4H). ^{13}C NMR (151 MHz, $CDCl_3$): δ 150.3, 129.7, 129.7, 112.7, 112.7, 112.7, 76.7, 76.7, 62.2, 52.8, 52.7, 46.8, 46.8, 40.8, 40.8, 24.0, 24.0. HRMS (ESI): *m/z* calculated for $C_{17}H_{27}N_3O$ 289.2153, found 290.2229 (M + H^+). Purity > 98%.

1-(5-Phenylfuran-2-yl)-N-((3-(pyrrolidin-1-yl)oxetan-3-yl)-methyl)methanamine (FTO-35 N). ^{1}H NMR (600 MHz, $CDCl_3$): δ 7.64 (d, *J* = 7.6 Hz, 2H), 7.37 (t, *J* = 7.8 Hz, 2H), 7.24 (t, *J* = 7.4 Hz, 1H), 6.58 (d, *J* = 3.3 Hz, 1H), 6.27 (d, *J* = 3.2 Hz, 1H), 4.78 (d, *J* = 6.6 Hz, 2H), 4.37 (d, *J* = 6.6 Hz, 2H), 3.88 (s, 2H), 3.01 (s, 2H), 2.67 (t, *J* = 5.9 Hz, 4H), 1.79−1.74 (m, 4H). ^{13}C NMR (151 MHz, $CDCl_3$): δ 153.7, 153.3, 128.8, 128.7, 128.7, 127.3, 123.6, 123.6, 109.5, 105.7, 77.0, 77.0, 62.6, 54.1, 46.8, 46.8, 46.2, 24.1, 24.1. HRMS (ESI): *m/z* calculated for $C_{19}H_{24}N_2O_2$ 312.1838, found 313.1910 (M + H^+). Purity > 97%.

1-(2-Butyl-5-chloro-1H-imidazol-4-yl)-N-((3-(pyrrolidin-1-yl)-oxetan-3-yl)methyl)methanamine (FTO-36 N). ^{1}H NMR (600 MHz, $CDCl_3$): δ 4.77 (d, *J* = 6.8 Hz, 2H), 4.35 (d, *J* = 6.8 Hz, 2H), 3.81 (s, 2H), 3.04 (s, 2H), 2.78 (t, *J* = 5.6, 4H), 2.63 (t, *J* = 8.1 Hz, 2H), 1.87−1.82 (m, 4H), 1.66 (m, 2H), 1.36 (dt, *J* = 14.9, 7.4 Hz, 2H), 0.91 (t, *J* = 7.4 Hz, 3H). ^{13}C NMR (151 MHz, $CDCl_3$): δ 147.4, 124.8, 121.7, 76.7, 76.7, 62.9, 54.3, 47.2, 47.2, 42.9, 30.4, 30.4, 28.7, 24.1, 22.4, 13.9. HRMS (ESI): *m/z* calculated for $C_{16}H_{27}ClN_4O$ 326.1873, found 327.1946 (M + H^+). Purity > 95%.

N-((1H-Indol-5-yl)methyl)-1-(3-(pyrrolidin-1-yl)oxetan-3-yl)-methanamine (FTO-37 N). ^{1}H (600 MHz, $CDCl_3$): δ 8.33 (s, 1H), 7.62 (d, *J* = 7.9 Hz, 1H), 7.36 (d, *J* = 8.2 Hz, 1H), 7.24 (d, *J* = 4.5 Hz, 1H), 7.20 (m, 1H), 7.11 (m, 1H), 4.79 (d, *J* = 6.6 Hz, 2H), 4.38 (d, *J* = 6.8 Hz, 2H), 3.83 (s, 2H), 3.07 (s, 2H), 2.80 (t, *J* = 5.8 Hz, 4H), 1.84 (t, *J* = 6.0 Hz, 4H). ^{13}C NMR (151 MHz, $CDCl_3$): δ 135.4, 128.1, 124.9, 122.8, 121.3, 120.8, 111.4, 102.6, 76.8, 76.8, 62.4, 54.0, 53.3, 46.8, 46.8, 24.0, 24.0. HRMS (ESI): *m/z* calculated for $C_{17}H_{23}N_3O$ 285.1841, found 286.1916 (M + H^+). Purity > 98%.

1-(5-Phenylthiophen-2-yl)-N-((3-(pyrrolidin-1-yl)oxetan-3-yl)-methyl)methanamine (FTO-38 N). ^{1}H NMR (600 MHz, $CDCl_3$): δ 7.58 (d, *J* = 7.0 Hz, 2H), 7.36 (t, *J* = 7.8 Hz, 2H), 7.26 (t, *J* = 7.1 Hz, 1H), 7.16 (d, *J* = 3.6 Hz, 1H), 6.89 (d, *J* = 3.6 Hz, 1H), 4.80 (t, *J* = 6.6 Hz, 2H), 4.39 (d, *J* = 6.6 Hz, 2H), 4.04 (s, 2H), 3.04 (s, 2H), 2.72 (t, *J* = 6.4 Hz, 4H), 1.82−1.78 (m, 4H). ^{13}C NMR (151 MHz, $CDCl_3$): δ 149.9, 143.6, 134.54, 129.0, 129.0, 127.4, 126.3, 125.7, 125.7, 122.7, 76.9, 76.9, 62.7, 53.9, 48.6, 47.0, 47.0, 25.4, 25.4. HRMS (ESI): *m/z* calculated for $C_{19}H_{24}N_2OS$ 328.1609, found 329.1683 (M + H^+). Purity > 95%.

1-(6-Methoxyquinolin-3-yl)-N-((3-(pyrrolidin-1-yl)oxetan-3-yl)-methyl)methanamine (FTO-39 N). ^{1}H NMR (600 MHz, $CDCl_3$): δ 8.75 (s, 1H), 8.02−7.96 (m, 2H), 7.34 (dt, *J* = 9.3, 2.6 Hz, 1H), 7.07 (s, 1H), 4.80 (d, *J* = 6.8 Hz, 2H), 4.37 (d, *J* = 6.8 Hz, 2H), 4.02 (s, 2H), 3.94 (s, 3H), 3.01 (s, 2H), 2.72 (q, *J* = 5.8 Hz, 4H), 1.84−1.76 (m, 4H). ^{13}C NMR (151 MHz, $CDCl_3$): δ 158.0, 149.1, 143.8, 133.8, 133.5, 130.7, 129.2, 121.9, 105.1, 77.0, 77.0, 62.8, 55.7, 54.8, 51.7, 47.0, 47.0, 24.1, 24.1. HRMS (ESI): *m/z* calculated for $C_{19}H_{25}N_3O_2$ 327.1947, found 328.2020 (M + H^+). Purity > 96%.

1-(3-(Pyrrolidin-1-yl)oxetan-3-yl)-N-(4-((trifluoromethyl)thio)-benzyl)methanamine (FTO-40 N). ^{1}H NMR (600 MHz, $CDCl_3$): δ 7.61 (d, *J* = 8.3 Hz, 2H), 7.40 (d, *J* = 8.4 Hz, 2H), 4.79 (d, *J* = 7.1 Hz, 2H), 4.36 (d, *J* = 6.7 Hz, 2H), 3.87 (s, 2H), 2.96 (s, 2H), 2.71 (t, *J* = 6.0 Hz, 4H), 1.82−1.77 (m, 4H). ^{13}C NMR (151 MHz, $CDCl_3$): δ 144.0, 136.6, 136.6, 130.8, 129.2, 129.2, 122.6, 77.0, 77.0, 62.7, 54.7, 53.5, 46.9, 46.9, 24.1, 24.1. HRMS (ESI): *m/z* calculated for $C_{16}H_{21}F_3N_2OS$ 346.1327, found 347.1401 (M + H^+). Purity > 97%.

1-(7-Methyl-1H-indol-3-yl)-N-((3-(pyrrolidin-1-yl)oxetan-3-yl)-methyl)methanamine (FTO-41 N). ^{1}H NMR (599 MHz, $CDCl_3$): δ 8.11 (s, 1H), 7.52 (d, *J* = 7.9 Hz, 1H), 7.17 (d, *J* = 2.4 Hz, 1H), 7.05 (t, *J* = 7.5 Hz, 1H), 7.00 (d, *J* = 7.1 Hz, 1H), 4.77 (d, *J* = 6.6 Hz, 2H), 4.37 (d, *J* = 6.6 Hz, 2H), 4.06 (s, 2H), 3.05 (s, 2H), 2.64 (t, *J* = 5.7 Hz, 4H), 2.49 (s, 3H), 1.77−1.69 (m, 4H). ^{13}C NMR (151 MHz, $CDCl_3$): δ 140.7, 136.1, 126.7, 122.8, 120.6, 119.9, 116.6, 114.8, 77.0, 77.0, 62.5, 54.4, 46.8, 46.8, 45.0, 24.0, 24.0, 16.8. HRMS (ESI): *m/z* calculated for $C_{18}H_{25}N_3O$ 299.1998, found 300.2072 (M + H^+). Purity > 96%.

1-(6-Methyl-1H-indol-3-yl)-N-((3-(pyrrolidin-1-yl)oxetan-3-yl)-methyl)methanamine (FTO-42 N). ^{1}H NMR (599 MHz, $CDCl_3$): δ 8.24 (s, 1H), 7.54 (d, *J* = 8.0 Hz, 1H), 7.15 (s, 1H), 7.08 (s, 1H), 6.96 (d, *J* = 8.1 Hz, 1H), 4.77 (d, *J* = 6.6 Hz, 2H), 4.38 (d, *J* = 6.6 Hz, 2H), 4.05 (s, 2H), 3.06 (s, 2H), 2.64 (t, *J* = 5.2 Hz, 4H), 2.46 (s, 3H), 1.77−1.69 (m, 4H). ^{13}C NMR (151 MHz, $CDCl_3$): δ 137.0, 132.0, 125.1, 122.5, 121.4, 118.5, 113.9, 111.3, 77.0, 77.0, 62.5, 54.3, 46.8, 46.8, 44.9, 24.0, 24.0, 21.8. HRMS (ESI): *m/z* calculated for $C_{18}H_{25}N_3O$ 299.1998, found 300.2072 (M + H^+). Purity > 96%.

1-(5-(2-Chlorophenyl)furan-2-yl)-N-((3-(pyrrolidin-1-yl)oxetan-3-yl)methyl)methanamine (FTO-43 N). ^{1}H NMR (599 MHz, $CDCl_3$): δ 7.91 (d, *J* = 8.1 Hz, 1H), 7.51 (d, *J* = 8.0 Hz, 1H), 7.38 (t, *J* = 7.6 Hz, 1H), 7.26 (t, *J* = 7.7 Hz, 1H), 7.15 (d, *J* = 3.6 Hz, 1H), 6.42 (d, *J* = 3.3 Hz, 1H), 4.87 (d, *J* = 6.6 Hz, 2H), 4.46 (d, *J* = 6.6 Hz, 2H), 3.99 (s, 2H), 3.11 (s, 2H), 2.77 (t, *J* = 5.5 Hz, 4H), 1.89−1.81 (m, 4H). ^{13}C NMR (151 MHz, $CDCl_3$): δ 153.7, 149.6, 130.8, 130.0, 129.2, 128.1, 127.7, 126.9, 111.8, 109.7, 76.9, 76.9, 62.7, 54.0, 46.9, 46.9, 46.2, 23.9, 23.9. HRMS (ESI): *m/z* calculated for $C_{19}H_{23}ClN_2O_2$ 346.1448, found 347.1520 (M + H^+). Purity > 99%.

1-(6-Fluoro-1H-indol-3-yl)-N-((3-(3-fluoropyrrolidin-1-yl)oxetan-3-yl)methyl)methanamine (FTO-44 N). ^{1}H NMR (599 MHz, $CDCl_3$): δ 8.32 (s, 1H), 7.58 (dd, *J* = 8.7, 5.3 Hz, 1H), 7.18 (s, 1H), 7.05 (d, *J* = 9.6 Hz, 1H), 6.92 (t, *J* = 9.1 Hz, 1H), 4.73 (dd, *J* = 12.4, 6.7 Hz, 2H), 4.39 (t, *J* = 7.7 Hz, 2H), 4.06 (s, 2H), 3.05 (s, 2H), 3.00 (t, *J* = 5.6 Hz, 1H), 2.98 (d, *J* = 3.1 Hz, 1H), 2.93 (d, *J* = 4.2 Hz, 1H), 2.85 (q, *J* = 8.1 Hz, 1H), 2.68 (td, *J* = 8.1, 3.8 Hz, 1H), 1.25 (s, 1H), 1.15 (d, *J* = 6.3 Hz, 1H). ^{13}C NMR (151 MHz, $CDCl_3$): δ 161.0, 159.4, 136.5, 123.8, 119.7, 108.7, 97.8, 94.0, 92.3, 76.8, 62.3, 54.0,

https://doi.org/10.1021/acs.jmedchem.1c02075
J. Med. Chem. 2022, 65, 10920−10937

53.9, 45.1, 44.6, 32.8, 29.8. HRMS (ESI): *m/z* calculated for $C_{17}H_{21}F_2N_3O$ 321.1653, found 322.1728 (M + H^+). Purity > 95%.

1-(5-Fluoro-1H-indol-3-yl)-N-((3-(3-fluoropyrrolidin-1-yl)oxetan-3-yl)methyl)methanamine (FTO-45 N). ^{1}H NMR (599 MHz, $CDCl_3$): δ 8.36 (s, 1H), 7.34−7.27 (m, 2H), 6.94 (t, *J* = 8.9 Hz, 1H), 4.75 (d, *J* = 6.8 Hz, 2H), 4.72 (d, *J* = 6.8 Hz, 2H), 4.40 (t, *J* = 7.2 Hz, 1H), 4.04 (s, 2H), 3.06 (s, 2H), 3.01−2.99 (m, 1H), 2.95 (d, *J* = 4.8 Hz, 1H), 2.87 (q, *J* = 8.1 Hz, 1H), 2.71 (td, *J* = 8.3, 3.7 Hz, 1H), 2.09−1.93 (m, 2H). ^{13}C NMR (151 MHz, $CDCl_3$): δ 158.7, 157.2, 133.0, 127.6, 125.2, 112.1, 110.9, 103.9, 93.9, 92.8, 76.8, 62.3, 54.1, 53.9, 45.4, 44.5, 32.6, 29.8. HRMS (ESI): *m/z* calculated for $C_{17}H_{21}F_2N_3O$ 321.1653, found 322.1730 (M + H^+). Purity > 97%.

1-(3-(3-Fluoropyrrolidin-1-yl)oxetan-3-yl)-N-((5-methyl-1H-indol-3-yl)methyl)methanamine (FTO-46 N). ^{1}H NMR (599 MHz, $CDCl_3$): δ 8.44 (s, 1H), 7.43 (s, 1H), 7.26 (d, *J* = 5.7 Hz, 1H), 7.22 (s, 1H), 7.03 (d, *J* = 8.2 Hz, 1H), 4.74 (d, *J* = 6.9 Hz, 2H), 4.71 (d, *J* = 7.0 Hz, 2H), 4.42 (t, *J* = 6.4 Hz, 2H), 4.15 (d, *J* = 3.2 Hz, 2H), 3.08 (d, *J* = 5.5 Hz, 2H), 2.99−2.93 (m, 1H), 2.93−2.87 (m, 1H), 2.80 (q, *J* = 8.2 Hz, 1H), 2.66 (td, *J* = 8.2, 3.8 Hz, 1H), 2.45 (s, 3H), 2.02−1.88 (m, 1H). ^{13}C NMR (151 MHz, $CDCl_3$): δ 134.9, 129.2, 127.4, 124.1, 124.0, 118.2, 111.2, 93.8, 92.7, 76.7, 62.1, 53.9, 53.0, 45.1, 44.3, 32.6, 29.8, 21.5. HRMS (ESI): *m/z* calculated for $C_{18}H_{24}FN_3O$ 317.1903, found 318.1978 (M + H^+). Purity > 96%.

N-((1H-Indol-3-yl)methyl)-1-(3-(3-fluoropyrrolidin-1-yl)oxetan-3-yl)methanamine (FTO-47 N). ^{1}H NMR (599 MHz, $CDCl_3$): δ 8.45 (s, 1H), 7.66 (d, *J* = 7.9 Hz, 1H), 7.38 (d, *J* = 8.1 Hz, 1H), 7.24 (d, *J* = 2.3 Hz, 1H), 7.21 (t, *J* = 7.5 Hz, 1H), 7.13 (t, *J* = 7.5 Hz, 1H), 4.74 (d, *J* = 6.9 Hz, 2H), 4.71 (d, *J* = 6.9 Hz, 2H), 4.41 (d, *J* = 6.9 Hz, 1H), 4.12 (s, 2H), 3.08 (s, 2H), 3.01−2.92 (m, 1H), 2.91 (t, *J* = 3.5 Hz, 1H), 2.82 (td, *J* = 8.7, 6.8 Hz, 1H), 2.67 (td, *J* = 8.2, 3.7 Hz, 1H), 2.04−1.96 (m, 2H). ^{13}C NMR (151 MHz, $CDCl_3$): δ 136.5, 127.1, 123.8, 122.4, 119.9, 118.7, 111.5, 93.9, 92.7, 76.7, 76.7, 62.2, 54.0, 53.4, 45.2, 44.4, 32.7. HRMS (ESI): *m/z* calculated for $C_{17}H_{22}FN_3O$ 303.1747, found 304.1821 (M + H^+). Purity > 95%.

1-(3-(3-Fluoropyrrolidin-1-yl)oxetan-3-yl)-N-((5-phenylfuran-2-yl)methyl)methanamine (FTO-48 N). ^{1}H NMR (599 MHz, $CDCl_3$): δ 7.65 (d, *J* = 8.3 Hz, 2H), 7.38 (t, *J* = 7.8 Hz, 2H), 7.25 (dd, *J* = 7.4, 1.3 Hz, 1H), 6.59 (d, *J* = 3.3 Hz, 1H), 6.28 (d, *J* = 3.2 Hz, 1H), 4.76 (dd, *J* = 14.4, 6.8 Hz, 2H), 4.41 (dd, *J* = 14.4, 6.8 Hz, 2H), 3.90 (s, 2H), 3.04 (d, *J* = 2.4 Hz, 1H), 3.01 (s, 2H), 2.98 (d, *J* = 3.8 Hz, 1H), 2.90 (q, *J* = 7.9 Hz, 1H), 2.74 (td, *J* = 8.2, 3.9 Hz, 1H), 2.14−1.90 (m, 3H). ^{13}C NMR (151 MHz, $CDCl_3$): δ 153.6, 130.9, 128.8, 128.8, 127.3, 123.6, 123.6, 109.6, 105.6, 94.0, 92.8, 76.8, 76.8, 62.5, 54.0, 53.8, 46.2, 45.1, 32.8. HRMS (ESI): *m/z* calculated for $C_{19}H_{23}FN_2O_2$ 330.1744, found 331.1817 (M + H^+). Purity > 98%.

1-(5-(2-Chlorophenyl)furan-2-yl)-N-((3-(3-fluoropyrrolidin-1-yl)-oxetan-3-yl)methyl)methanamine (FTO-49 N). ^{1}H NMR (599 MHz, $CDCl_3$): δ 7.82 (d, *J* = 7.9 Hz, 1H), 7.42 (d, *J* = 8.0 Hz, 1H), 7.30 (t, *J* = 7.6 Hz, 1H), 7.18 (t, *J* = 7.6 Hz, 1H), 7.07 (d, *J* = 3.4 Hz, 1H), 6.34 (d, *J* = 3.3 Hz, 1H), 4.75 (dd, *J* = 15.9, 6.8 Hz, 2H), 4.41 (dd, *J* = 15.7, 6.8 Hz, 2H), 3.90 (s, 2H), 3.02 (d, *J* = 6.7 Hz, 1H), 3.02 (s, 2H), 2.98−2.96 (m, 1H), 2.89 (dt, *J* = 9.5, 7.8 Hz, 1H), 2.73 (td, *J* = 8.3, 4.0 Hz, 1H), 2.11−1.94 (m, 3H). ^{13}C NMR (151 MHz, $CDCl_3$): δ 153.56, 149.6, 130.9, 130.0, 129.2, 128.0, 127.7, 127.0, 111.8, 109.7, 93.9, 92.8, 76.8, 62.4, 54.0, 53.7, 46.0, 45.2, 32.8. HRMS (ESI): *m/z* calculated for $C_{19}H_{22}ClFN_2O_2$ 364.1354, found 365.1427 (M + H^+). Purity > 99%.

1-(3-(3-Fluoropyrrolidin-1-yl)oxetan-3-yl)-N-((8-methylquinolin-3-yl)methyl)methanamine (FTO-50 N). ^{1}H NMR (599 MHz, $CDCl_3$): δ 8.95 (d, *J* = 1.2 Hz, 1H), 8.08 (s, 1H), 7.67 (d, *J* = 8.1 Hz, 1H), 7.56 (d, *J* = 7.0 Hz, 1H), 7.45 (t, *J* = 7.6 Hz, 1H), 5.20 (s, 1H), 4.77 (dd, *J* = 15.1, 6.8 Hz, 2H), 4.41 (dd, *J* = 18.4, 6.8 Hz, 2H), 4.06 (s, 2H), 3.07 (d, *J* = 3.2 Hz, 1H), 3.04−2.94 (m, 4H), 2.84 (s, 3H), 2.80 (td, *J* = 8.3, 3.9 Hz, 1H), 2.15−2.08 (m, 3H). ^{13}C NMR (151 MHz, $CDCl_3$): δ 150.4, 146.7, 137.0, 135.0, 132.6, 129.5, 128.0, 126.7, 125.8, 93.9, 92.8, 76.8, 62.6, 54.3, 51.5, 45.3, 32.8, 18.3. HRMS (ESI): *m/z* calculated for $C_{19}H_{24}FN_3O$ 329.1903, found 330.1978 (M + H^+). Purity > 98%.

1-(5-(2-Chloro-5-(trifluoromethyl)phenyl)furan-2-yl)-N-((3-(pyrrolidin-1-yl)oxetan-3-yl)methyl)methanamine (FTO-51 N). ^{1}H NMR (599 MHz, $CDCl_3$): δ 8.08 (s, 1H), 7.53 (d, *J* = 8.4 Hz, 1H), 7.40 (d, *J* = 8.4 Hz, 1H), 7.17 (d, *J* = 3.4 Hz, 1H), 6.37 (d, *J* = 3.4 Hz, 1H), 4.79 (d, *J* = 6.7 Hz, 2H), 4.37 (d, *J* = 6.7 Hz, 2H), 3.92 (s, 2H), 3.03 (s, 2H), 2.71 (t, *J* = 6.1 Hz, 4H), 1.81−1.74 (m, 4H). ^{13}C NMR (151 MHz, $CDCl_3$): δ 154.8, 148.1, 133.1, 131.5, 129.9, 129.5 (q, CF_3), 124.4, 124.1, 122.9, 113.2, 109.9, 76.9, 76.9, 62.7, 54.2, 46.9, 46.9, 46.2, 24.0, 24.0. HRMS (ESI): *m/z* calculated for $C_{20}H_{22}ClF_3N_2O_2$ 414.1322, found 415.1393 (M + H^+). Purity > 98%.

1-(5-(3-Chloro-4-methoxyphenyl)furan-2-yl)-N-((3-(pyrrolidin-1-yl)oxetan-3-yl)methyl)methanamine (FTO-52 N). ^{1}H NMR (599 MHz, $CDCl_3$): δ 7.64 (d, *J* = 2.2 Hz, 1H), 7.48 (d, *J* = 8.6 Hz, 1H), 6.92 (dd, *J* = 8.6, 2.0 Hz, 1H), 6.46 (s, 1H), 6.25 (s, 1H), 4.78 (dd, *J* = 6.7, 1.9 Hz, 2H), 4.37 (dd, *J* = 6.7, 1.9 Hz, 2H), 3.94 (d, *J* = 1.9 Hz, 3H), 3.91 (s, 2H), 3.00 (s, 2H), 2.69 (t, *J* = 5.3 Hz, 4H), 1.81−1.73 (m, 4H). ^{13}C NMR (151 MHz, $CDCl_3$): δ 154.2, 153.4, 152.0, 125.7, 124.9, 123.1, 122.9, 112.3, 109.6, 105.0, 76.9, 76.9, 62.6, 56.3, 54.0, 46.8, 46.8, 46.2, 24.1, 24.1. HRMS (ESI): *m/z* calculated for $C_{20}H_{25}ClN_2O_3$ 376.1554, found 377.1626 (M + H^+). Purity > 98%.

1-(5-(3,4-Dichlorophenyl)furan-2-yl)-N-((3-(pyrrolidin-1-yl)-oxetan-3-yl)methyl)methanamine (FTO-53 N). ^{1}H NMR (599 MHz, $CDCl_3$): δ 7.71 (d, *J* = 1.9 Hz, 1H), 7.43 (td, *J* = 6.0, 1.9 Hz, 1H), 7.41 (d, *J* = 8.4 Hz, 1H), 6.60 (d, *J* = 3.3 Hz, 1H), 6.29 (d, *J* = 3.3 Hz, 1H), 4.78 (d, *J* = 6.7 Hz, 2H), 4.36 (d, *J* = 6.7 Hz, 2H), 3.88 (s, 2H), 3.00 (s, 2H), 2.70 (t, *J* = 6.4 Hz, 4H), 1.82−1.75 (m, 4H). ^{13}C NMR (151 MHz, $CDCl_3$): δ 154.7, 150.9, 133.0, 130.8, 130.8, 130.8, 125.3, 122.8, 109.8, 107.3, 76.9, 76.9, 62.7, 54.1, 46.9, 46.9, 46.3, 24.1, 24.1. HRMS (ESI): *m/z* calculated for $C_{19}H_{22}Cl_2N_2O_2$ 380.1058, found 381.1130 (M + H^+). Purity > 99%.

Cell Culture Methods. AGS (CRL-1739; Human Gastric Adenocarcinoma), SNU-16 (CRL-5974; Human Gastric Carcinoma), and KATOIII (HTB-103; Human Gastric Carcinoma) were all purchased from the American Type Culture Collection (ATCC). These cell lines were cultured in F-12K medium (ATCC, 30-2004), RPMI-1640 (ATCC, 30-2001) and IMDM (ATCC, 30-2005), respectively. HEK293T cells and MRC-5 cells were cultured in DMEM. U937 cells, NB4 cells, and THP-1 cells were cultured in RPMI-1640 (Gibco), and CCD 841 CoN cells were cultured in Eagle's minimum essential medium (EMEM) (ATCC, 30−2003). All media were supplemented with 10% fetal bovine serum (Gibco). All cells were cultured at 37 °C in a humidified 5% CO_2 atmosphere.

Cell Viability Assays. The procedures were approved by the University of California San Diego Institutional Review Board. To evaluate the antiproliferative effects of FTO inhibitors in various cancerous and noncancerous cell lines, cytotoxicity was measured using a Cell Counting Kit-8 (CCK-8) assay (Apexbio Technology LLC K1018, Fisher Scientific 50-190-5564) following the manufacturer's instructions. The evaluation of FTO inhibitors was performed in glioblastoma cells (U87, A172, T98, TS576, GSC23, and GBM6), gastric cancer cells (AGS, SNU-16, KATOIII), acute myeloid leukemia cells (U937, THP-1, NB4), and normal epithelial cells (CCD 841). GSC23, GBM6, and TS576 cell lines were obtained from the Frank Furnari lab at UCSD and cultured in DMEM/F12 medium supplemented with 1:100 B27 without vitamin A, EGF (20 ng/mL), FGF (10 ng/mL), and penicillin−streptomycin (100 IU/mL) as previously described.[11,12]

A total of 10,000 cells were plated in 96-well plates for cell viability assays. Initial screening was performed for a single dose of 30 μM 48 h post-exposure. Tested cell lines were exposed to a series of concentrations (0, 5, 10, 20, 25, and 50 μM) of FTO-43 N for 24, 48, and 72 h. All data were normalized to culture medium for background control. Two hours before the end of the culture period, 10 μL of CCK-8 was added to each well including medium-only wells (blanks). After 2 h of incubation with CCK-8 at 37 °C, the optical density of the viable cells was recorded at 450 nm using a BioTek Synergy plate reader. Relative cell viability was expressed as a percentage relative to the DMSO treated control cells and 0 time points. FTO knockdown cell lines were expressed as a percentage-relative shRNA control (shNTC). Each experiment was repeated three times and performed in triplicate or quadruplicate.

https://doi.org/10.1021/acs.jmedchem.1c02075
J. Med. Chem. 2022, 65, 10920−10937

Lentiviral Generation and Infection. Lentiviral particles were prepared for shControl, shFTO1, and shFTO2 as previously described in Huff *et al.*[8] Lentiviruses were generated by co-transfecting HEK293T cells with the shRNA-expressing vectors (carrying a puromycin resistance gene), a packaging plasmid (psPAX2), and an envelope plasmid (pMD2.G) using Opti-MEM and Lipofectamine 3000 (Life Technologies, 11,668,027) according to the manufacturer's instructions. The medium was replaced with fresh completed DMEM after 4−6 h. The virus-containing supernatant was harvested after 48 h of transduction, filtered at 0.45 μm, and stored at −80 °C. Generated shRNA control (NTC), shFTO-249, and shFTO-250 lentivirus particles were used to infect AGS cells, SNU-16 cells, and KATOIII cells in the presence of Polybrene (8 μg/mL) (Millipore) by spin transduction (centrifuge at 750*g* for 45 min at RT). After 12 h of infection, the lentivirus-containing medium was replaced with fresh medium, and transduced cells were selected by culture with puromycin (Sigma TR-1003) at 1.5 μg/mL for AGS and SNU-16, 4 ug/ml for KATOIII for 7 days to generate TFO knock down (KD) stable cell lines, and KD efficiency was determined by qPCR or Western blot analysis.

Immunoblotting. Proteins from cells were extracted using Pierce IP Lysis Buffer supplemented with protease inhibitors (Life Technologies, 87786) followed by centrifugation to remove insoluble material, and clarified supernatant was measured using a BCA protein assay kit (Bio-Rad). Thirty micrograms of protein was resolved by NuPAGE 4−12% Bis-Tris gels and transferred to PVDF membranes (Bio-Rad) according to the manufacturer's instructions. Membranes were blocked in 5% non-fat dry milk in PBS buffer and then incubated with the indicated antibodies including FTO (Cell Signaling Technology, 14386), GAPDH (Proteintech, HRP-60004), Axin1 (Cell Signaling Technology, 2087), β-catenin (Cell Signaling Technology, 8480), Akt (Cell Signaling Technology, 4691), Phospho-Akt (Ser473) (Cell Signaling Technology, 4060) and E-cadherin (Cell Signaling Technology, 3195) overnight at 4 °C. After being washed, the membranes were incubated with HRP-conjugated secondary antibodies at room temperature (RT) for 15 min and then washed 3 times as before (Thermo Scientific, Pierce Fast Western Blotting Blot Kit). Protein was visualized on autoradiography film (Genesee Scientific Inc., 30-100) using the enhanced chemiluminescence (ECL) detection system (Thermo Scientific).

RNA Isolation. Total RNA was extracted from culture cells using Direct-zol RNA MiniPrep Kit (Zymo Research, 11−331); all RNAs were treated with DNase I. mRNA was isolated using the Magnetic mRNA Isolation Kit (New England Biolabs, S1550S) following the manufacturer's instructions.

Quantitative Real-Time PCR. Reverse transcription of total RNA to cDNA was performed using the iScript Reverse Transcription Synthesis Kit (Bio-Rad, 1,708,841), and qPCR reactions were set up in 10 μL volumes, consisting of 3 μL of cDNA (6−15 ng), 2 μL of mixed forward and reverse (300 nM) primers and 5 μL of SsoAdvanced Universal SYBR Green PCR SuperMix (Bio-Rad, 1725270). qPCR was run on 384 well-PCR machine. The primers used in this study were listed below. The transcript level of *FTO* was quantified using the ΔΔ Ct method using *GAPDH* as a housekeeping reference gene.

FTO forward: 5′-TTGCCCGAACATTACCTGCT-3′.

FTO reverse: 5′-TGTGAGGTCAAACGGCAGAG-3′.

m^{6}A Dot-Blot Assay. m^{6}A dot-blot assays were performed as described in Huff *et al.*[29] mRNA or total RNA were isolated from AGS cells treated with either shControl, shFTO1, shFTO2, DMSO, or FTO-43 N using Magnetic mRNA Isolation Kit (New England Biolabs, S1550S). RNA samples were quantified, serially diluted, and denatured at 95 °C for 3 min and then chilled on ice to prevent the reformation of the secondary structure of mRNA. Denatured mRNA samples were spotted on an Amersham Hybond-N+ membrane (GE Healthcare, RPN3050B) and cross-linked to the membrane with UV radiation. After cross-linking, the membrane was washed with phosphate-buffered saline with 0.02% Tween 20 (PBST), blocked in 5% non-fat milk in PBST buffer for 1 h at room temperature (RT), and then incubated with anti-m^{6}A antibody (1: 1000; Abcam) overnight at 4 °C. The membrane was then washed as before and incubated in HRP-conjugated secondary antibodies for 1 h at RT. The signaling was detected by SuperSignal West Pico Chemiluminescent Substrate (Thermo Scientific, 34080) and developed using autoradiography film (Genesee Scientific Inc., 30-100). For RNA loading control, after imaging, the membrane was stained with 0.2% methylene blue in 0.4 M sodium acetate and 0.4 M acetic acid for 1 h and washed with water for until the background is clean.

Statistical Analysis. All values are expressed as the means ± SEM of at least three independent experiments if no additional information was indicated. Statistical differences among groups were determined using either Student's *t* test or one-way ANOVA. *P* values of less than 0.05 were considered statistically significant. The analyses were performed using GraphPad Prism 8 software.

Quantification of m^{6}A and m^{6}A$_m$ by LC−MS/MS/MS. Polyadenylated RNA was analyzed by LC−MS/MS/MS as described previously.[13,29] Briefly, polyadenylated RNA (100 ng) was incubated with 5 units of RppH in ThermoPol buffer at 37 °C for 3 h. The mixture was then digested with 1 unit of nuclease P1 in 25 μL buffer containing 25 mM of NaCl and 2.5 mM of $ZnCl_2$ at 37 °C for 2 h followed by the addition of 3 μL of 1 M NH_4HCO_3 and 1 U alkaline phosphatase. After an additional incubation at 37 °C for 2 h, uniformly ^{15}N-labeled rA and D_3-labeled m^{6}A internal standards were added to the mixture. The enzymes in the digestion mixture were removed by extraction with chloroform, and the salts in the digestion mixture were removed by CH_3CN precipitation. The ensuing supernatant was dried by Speed-vac, redissolved in doubly distilled water, and subjected to LC−MS/MS analysis.

The LC−MS/MS/MS experiments were conducted on an LTQ-XL linear ion trap mass spectrometer (Thermo Fisher Scientific) coupled with an EASY-nLC II system (Thermo Fisher Scientific). Mobile phase A was 0.1% formic acid in H_2O, and mobile phase B was 0.1% formic acid in acetonitrile. The samples were loaded onto a trapping column (150 μm i.d.) packed with porous graphitic carbon (PGC, 5 μm particle size, Thermo Fisher Scientific) at a flow rate of 2.5 μL/min within 8 min. The samples were then eluted onto an analytical column (75 μm i.d.) packed with Zorbax SB-C18 (5 μm in particle size, 100 Å in pore size, Agilent) using a nonlinear gradient consisting of 0−16% B in 5 min, 16−22% B in 23 min, 22−50% B in 17 min, 50−90% B in 5 min, and finally at 90% B for 30 min at a flow rate of 300 nL/min. Quantification was performed by comparison with the calibration curves obtained from pure nucleoside standards analyzed under the same experimental conditions. Based on the peak area ratios in the selected-ion chromatograms for the analytes over their corresponding isotope-labeled standards, the amounts of the labeled standards added and the equations derived from the calibration curves, the moles of m^{6}A, m^{6}A$_m$, and rA in the nucleoside mixtures were calculated. The amounts of m^{6}A and m^{6}A$_m$ were normalized to that of rA in the same sample to give the levels of these two modified nucleosides.

■ ASSOCIATED CONTENT

Supporting Information

The Supporting Information is available free of charge at https://pubs.acs.org/doi/10.1021/acs.jmedchem.1c02075.

Expanded synthetic methods and spectra for FTO-01−50 N; calculated physicochemical properties for oxetane inhibitors and FDA-approved CNS drugs; docking poses for select compounds; demethylation assay controls and velocity plots for select FTO inhibitors; lentiviral knockdown efficiency, time-dependent growth inhibition in gastric cancer cells, and m^{6}A RNA dot-blot assays (PDF)

Molecular formula strings (CSV)

https://doi.org/10.1021/acs.jmedchem.1c02075
J. Med. Chem. 2022, 65, 10920−10937

AUTHOR INFORMATION

Corresponding Author

Tariq M. Rana − *Division of Genetics, Department of Pediatrics, Center for Drug Discovery Innovation, Program in Immunology, Institute for Genomic Medicine, University of California San Diego, La Jolla, California 92093, United States; San Diego Center for Precision Immunotherapy, Moores Cancer Center 3855 Health Sciences Drive, University of California San Diego, La Jolla, California 92093, United States;* orcid.org/0000-0001-9558-5766; Email: trana@ucsd.edu

Authors

Sarah Huff − *Division of Genetics, Department of Pediatrics, Center for Drug Discovery Innovation, Program in Immunology, Institute for Genomic Medicine, University of California San Diego, La Jolla, California 92093, United States*

Indrasena Reddy Kummetha − *Division of Genetics, Department of Pediatrics, Center for Drug Discovery Innovation, Program in Immunology, Institute for Genomic Medicine, University of California San Diego, La Jolla, California 92093, United States*

Lingzhi Zhang − *Division of Genetics, Department of Pediatrics, Center for Drug Discovery Innovation, Program in Immunology, Institute for Genomic Medicine, University of California San Diego, La Jolla, California 92093, United States*

Lingling Wang − *Division of Genetics, Department of Pediatrics, Center for Drug Discovery Innovation, Program in Immunology, Institute for Genomic Medicine, University of California San Diego, La Jolla, California 92093, United States*

William Bray − *Division of Genetics, Department of Pediatrics, Center for Drug Discovery Innovation, Program in Immunology, Institute for Genomic Medicine, University of California San Diego, La Jolla, California 92093, United States;* orcid.org/0000-0003-2414-0190

Jiekai Yin − *Environmental Toxicology Graduate Program and Department of Chemistry, University of California, Riverside, California 92521, United States*

Vanessa Kelley − *Division of Genetics, Department of Pediatrics, Center for Drug Discovery Innovation, Program in Immunology, Institute for Genomic Medicine, University of California San Diego, La Jolla, California 92093, United States*

Yinsheng Wang − *Environmental Toxicology Graduate Program and Department of Chemistry, University of California, Riverside, California 92521, United States*

Complete contact information is available at: https://pubs.acs.org/10.1021/acs.jmedchem.1c02075

Author Contributions

‖S.H. and I.R.K. contributed equally to this work.

Author Contributions

S.H. designed and performed the experiments, analyzed the data, and wrote the manuscript. I.R.K., L.Z., L.W., W.B., J. Y., V.K. performed experiments analyzed the data and prepared the figures. Y.W. supervised MS experiments, analyzed the MS data, and edited the manuscript. T.M.R. conceived and planned the project, and participated in experimental design, data analysis, data interpretation, and manuscript writing.

Notes

The authors declare the following competing financial interest(s): TMR is a co-founder and has equity interest in Gibraltar Sciences, a company dedicated to developing targeted molecular and immunotherapies for untreatable cancers. The terms of this arrangement have been reviewed and approved by the University of California, San Diego in accordance with its conflict of interest policies.

ACKNOWLEDGMENTS

We thank Dr. Frank Furnari for the GBM cell lines and Dr. Samie Jaffrey for providing ALKBH5 and FTO plasmids for protein expression and purification. The authors thank Dr. Dionicio Siegel and Brendan Duggan of UCSD Skaggs School of Pharmacy for assistance with synthetic chemistry and NMR spectroscopy. The authors thank Sarah Stumpf for her assistance with the *in vitro* inhibition assays. We also thank members of the Rana lab for helpful discussions and advice. This work was supported in part by grants from the National Institutes of Health and a T32 fellowship to S.H. (award number T32 CA121938).

ABBREVIATIONS

5FU, 5-fluorourcil; ADME, adsorption, distribution, metabolism, and excretion; ALKBH5, m^6A RNA demethylase ALKBH5; AML, acute myeloid leukemia; ANOVA, analysis of variance; B-PER, bacterial protein extraction reagent; cDNA, complementary DNA; CNS, central nervous system; DCM, dichloromethane; DMEM, Dulbecco's modified Eagle medium; DMSO, dimethyl sulfoxide; DNase I, deoxyribonuclease I; ECL, enhanced chemiluminescence; EMEM, Eagle's minimum essential medium; EtOAc, ethyl acetate; F-12K, Kaighn's modification of Ham's F-12 medium; FDA, Federal Drug Administration; FITC, fluorescein isothiocyanate; FTO, fat mass- and obesity-associated protein; GBM, glioblastoma multiforme; GSCs, glioblastoma stem cells, GTex, genotype-tissue expression; hNSCs, healthy neural stem cells; HPLC, high-performance liquid chromatography; HPLC-MS/MS/MS, high-performance liquid chromatography−tandem mass spectrometry; HRMS, high-resolution mass spectrometry; HRP, horseradish peroxidase; IMDM, Iscove's modified Dulbecco's medium; IPTG, isopropyl β-D-1-thiogalactopyranoside; LB, Luria broth; LLE, lipophilic ligand efficiency; log*D*, logarithm of partition of a compound between octanol and PBS (pH 7.4); m^6A, N^6-methyladenosine RNA; m^6A_m, N^6-2′-*O*-dimethyladenosine; MeOH, methanol; METTL3, methyltransferase 3, N^6-adenosine-methyltransferase complex catalytic subunit; METTL14, methyltransferase 14, N^6-adenosine-methyltransferase subunit; MFA, meclofenamic acid; mRNA, messenger RNA; NMR, nuclear magnetic resonance; OPLS, Optimized Potentials for Liquid Simulations All-Atom; PBST, 1× phosphate-buffered saline, 0.1% Tween 20; pIC_{50}, negative logarithm of IC_{50}; PK, pharmacokinetic; PVDF, polyvinylidene fluoride; qPCR, quantitative polymerase chain reaction; RPMI-1640, Roswell Park Memorial Institute medium; RppH, RNA 5′ polyhydrolase; RT, room temperature; SEM, standard error of the mean; SGB, surface-generalized Born; shRNA, short hairpin RNA; TBST, Tris-buffered saline, 0.1% Tween 20; TCGA, The Cancer Genome Atlas; THF, tetrahydrofuran; v_{max}, maximum reaction velocity; WTAP, WT1-associated protein; YTHDC1−2, YTH domain-containing family proteins 1−2; YTHDF1−3, YTH domain-containing family proteins 1−3

https://doi.org/10.1021/acs.jmedchem.1c02075
J. Med. Chem. 2022, 65, 10920−10937

REFERENCES

(1) Dominissini, D.; Moshitch-Moshkovitz, S.; Schwartz, S.; Salmon-Divon, M.; Ungar, L.; Osenberg, S.; Cesarkas, K.; Jacob-Hirsch, J.; Amariglio, N.; Kupiec, M.; Sorek, R.; Rechavi, G. Topology of the human and mouse m6A RNA methylomes revealed by m6A-seq. *Nature* **2012**, *485*, 201−206.

(2) Frye, M.; Harada, B. T.; Behm, M.; He, C. RNA modifications modulate gene expression during development. *Science* **2018**, *361*, 1346−1349.

(3) Meyer, K. D.; Patil, D. P.; Zhou, J.; Zinoviev, A.; Skabkin, M. A.; Elemento, O.; Pestova, T. V.; Qian, S. B.; Jaffrey, S. R. 5′ UTR m(6)A Promotes Cap-Independent Translation. *Cell* **2015**, *163*, 999−1010.

(4) Wang, X.; He, C. Dynamic RNA modifications in posttranscriptional regulation. *Mol. Cell* **2014**, *56*, 5−12.

(5) Liu, J.; Yue, Y.; Han, D.; Wang, X.; Fu, Y.; Zhang, L.; Jia, G.; Yu, M.; Lu, Z.; Deng, X.; Dai, Q.; Chen, W.; He, C. A METTL3-METTL14 complex mediates mammalian nuclear RNA N6-adenosine methylation. *Nat. Chem. Biol.* **2014**, *10*, 93−95.

(6) Wang, X.; Feng, J.; Xue, Y.; Guan, Z.; Zhang, D.; Liu, Z.; Gong, Z.; Wang, Q.; Huang, J.; Tang, C.; Zou, T.; Yin, P. Structural basis of N(6)-adenosine methylation by the METTL3-METTL14 complex. *Nature* **2016**, *534*, 575−578.

(7) Kasowitz, S. D.; Ma, J.; Anderson, S. J.; Leu, N. A.; Xu, Y.; Gregory, B. D.; Schultz, R. M.; Wang, P. J. Nuclear m6A reader YTHDC1 regulates alternative polyadenylation and splicing during mouse oocyte development. *PLoS Genet.* **2018**, *14*, No. e1007412.

(8) Wang, X.; Zhao, B. S.; Roundtree, I. A.; Lu, Z.; Han, D.; Ma, H.; Weng, X.; Chen, K.; Shi, H.; He, C. N(6)-methyladenosine Modulates Messenger RNA Translation Efficiency. *Cell* **2015**, *161*, 1388−1399.

(9) Shi, H.; Wang, X.; Lu, Z.; Zhao, B. S.; Ma, H.; Hsu, P. J.; Liu, C.; He, C. YTHDF3 facilitates translation and decay of N(6)-methyladenosine-modified RNA. *Cell Res* **2017**, *27*, 315−328.

(10) Zaccara, S.; Jaffrey, S. R. A Unified Model for the Function of YTHDF Proteins in Regulating m(6)A-Modified mRNA. *Cell* **2020**, *181*, 1582−1595.

(11) Han, Z.; Niu, T.; Chang, J.; Lei, X.; Zhao, M.; Wang, Q.; Cheng, W.; Wang, J.; Feng, Y.; Chai, J. Crystal structure of the FTO protein reveals basis for its substrate specificity. *Nature* **2010**, *464*, 1205−1209.

(12) Jia, G.; Fu, Y.; Zhao, X.; Dai, Q.; Zheng, G.; Yang, Y.; Yi, C.; Lindahl, T.; Pan, T.; Yang, Y. G.; He, C. N6-methyladenosine in nuclear RNA is a major substrate of the obesity-associated FTO. *Nat. Chem. Biol.* **2011**, *7*, 885−887.

(13) Zheng, G.; Dahl, J. A.; Niu, Y.; Fedorcsak, P.; Huang, C. M.; Li, C. J.; Vagbo, C. B.; Shi, Y.; Wang, W. L.; Song, S. H.; Lu, Z.; Bosmans, R. P.; Dai, Q.; Hao, Y. J.; Yang, X.; Zhao, W. M.; Tong, W. M.; Wang, X. J.; Bogdan, F.; Furu, K.; Fu, Y.; Jia, G.; Zhao, X.; Liu, J.; Krokan, H. E.; Klungland, A.; Yang, Y. G.; He, C. ALKBH5 is a mammalian RNA demethylase that impacts RNA metabolism and mouse fertility. *Mol. Cell* **2013**, *49*, 18−29.

(14) Mauer, J.; Jaffrey, S. R. FTO, m(6) Am , and the hypothesis of reversible epitranscriptomic mRNA modifications. *FEBS Lett.* **2018**, *592*, 2012−2022.

(15) Mauer, J.; Luo, X.; Blanjoie, A.; Jiao, X.; Grozhik, A. V.; Patil, D. P.; Linder, B.; Pickering, B. F.; Vasseur, J. J.; Chen, Q.; Gross, S. S.; Elemento, O.; Debart, F.; Kiledjian, M.; Jaffrey, S. R. Reversible methylation of m6Am in the 5′ cap controls mRNA stability. *Nature* **2017**, *541*, 371−375.

(16) Mauer, J.; Sindelar, M.; Despic, V.; Guez, T.; Hawley, B. R.; Vasseur, J. J.; Rentmeister, A.; Gross, S. S.; Pellizzoni, L.; Debart, F.; Goodarzi, H.; Jaffrey, S. R. FTO controls reversible m(6)Am RNA methylation during snRNA biogenesis. *Nat. Chem. Biol.* **2019**, *15*, 340−347.

(17) Wei, J.; Liu, F.; Lu, Z.; Fei, Q.; Ai, Y.; He, P. C.; Shi, H.; Cui, X.; Su, R.; Klungland, A.; Jia, G.; Chen, J.; He, C. Differential m(6)A, m(6)Am, and m(1)A Demethylation Mediated by FTO in the Cell Nucleus and Cytoplasm. *Mol. Cell* **2018**, *71*, 973−985.e5.

(18) Koh, C. W. Q.; Goh, Y. T.; Goh, W. S. S. Atlas of quantitative single-base-resolution N(6)-methyl-adenine methylomes. *Nat. Commun.* **2019**, *10*, 5636.

(19) Boriack-Sjodin, P. A.; Ribich, S.; Copeland, R. A. RNA-modifying proteins as anticancer drug targets. *Nat. Rev. Drug. Discov.* **2018**, *17*, 435−453.

(20) Panneerdoss, S.; Eedunuri, V. K.; Yadav, P.; Timilsina, S.; Rajamanickam, S.; Viswanadhapalli, S.; Abdelfattah, N.; Onyeagucha, B. C.; Cui, X.; Lai, Z.; Mohammad, T. A.; Gupta, Y. K.; Huang, T. H.; Huang, Y.; Chen, Y.; Rao, M. K. Cross-talk among writers, readers, and erasers of m(6)A regulates cancer growth and progression. *Sci. Adv.* **2018**, *4*, No. eaar8263.

(21) Zhang, C.; Samanta, D.; Lu, H.; Bullen, J. W.; Zhang, H.; Chen, I.; He, X.; Semenza, G. L. Hypoxia induces the breast cancer stem cell phenotype by HIF-dependent and ALKBH5-mediated m(6)A-demethylation of NANOG mRNA. *Proc. Natl. Acad. Sci. U. S. A.* **2016**, *113*, E2047−E2056.

(22) Barbieri, I.; Tzelepis, K.; Pandolfini, L.; Shi, J.; Millan-Zambrano, G.; Robson, S. C.; Aspris, D.; Migliori, V.; Bannister, A. J.; Han, N.; De Braekeleer, E.; Ponstingl, H.; Hendrick, A.; Vakoc, C. R.; Vassiliou, G. S.; Kouzarides, T. Promoter-bound METTL3 maintains myeloid leukaemia by m(6)A-dependent translation control. *Nature* **2017**, *552*, 126−131.

(23) Cui, Q.; Shi, H.; Ye, P.; Li, L.; Qu, Q.; Sun, G.; Sun, G.; Lu, Z.; Huang, Y.; Yang, C. G.; Riggs, A. D.; He, C.; Shi, Y. m6A RNA Methylation Regulates the Self-Renewal and Tumorigenesis of Glioblastoma Stem Cells. *Cell Rep.* **2017**, *18*, 2622−2634.

(24) Su, R.; Dong, L.; Li, C.; Nachtergaele, S.; Wunderlich, M.; Qing, Y.; Deng, X.; Wang, Y.; Weng, X.; Hu, C.; Yu, M.; Skibbe, J.; Dai, Q.; Zou, D.; Wu, T.; Yu, K.; Weng, H.; Huang, H.; Ferchen, K.; Qin, X.; Zhang, B.; Qi, J.; Sasaki, A. T.; Plas, D. R.; Bradner, J. E.; Wei, M.; Marcucci, G.; Jiang, X.; Mulloy, J. C.; Jin, J.; He, C.; Chen, J. R-2HG Exhibits Anti-tumor Activity by Targeting FTO/m(6)A/MYC/CEBPA Signaling. *Cell* **2018**, *172*, 90−105.e23.

(25) Vu, L. P.; Pickering, B. F.; Cheng, Y.; Zaccara, S.; Nguyen, D.; Minuesa, G.; Chou, T.; Chow, A.; Saletore, Y.; MacKay, M.; Schulman, J.; Famulare, C.; Patel, M.; Klimek, V. M.; Garrett-Bakelman, F. E.; Melnick, A.; Carroll, M.; Mason, C. E.; Jaffrey, S. R.; Kharas, M. G. The N(6)-methyladenosine (m(6)A)-forming enzyme METTL3 controls myeloid differentiation of normal hematopoietic and leukemia cells. *Nat. Med.* **2017**, *23*, 1369−1376.

(26) Huang, Y.; Su, R.; Sheng, Y.; Dong, L.; Dong, Z.; Xu, H.; Ni, T.; Zhang, Z. S.; Zhang, T.; Li, C.; Han, L.; Zhu, Z.; Lian, F.; Wei, J.; Deng, Q.; Wang, Y.; Wunderlich, M.; Gao, Z.; Pan, G.; Zhong, D.; Zhou, H.; Zhang, N.; Gan, J.; Jiang, H.; Mulloy, J. C.; Qian, Z.; Chen, J.; Yang, C. G. Small-Molecule Targeting of Oncogenic FTO Demethylase in Acute Myeloid Leukemia. *Cancer Cell* **2019**, *35*, 677−691.e10.

(27) Li, Z.; Weng, H.; Su, R.; Weng, X.; Zuo, Z.; Li, C.; Huang, H.; Nachtergaele, S.; Dong, L.; Hu, C.; Qin, X.; Tang, L.; Wang, Y.; Hong, G. M.; Huang, H.; Wang, X.; Chen, P.; Gurbuxani, S.; Arnovitz, S.; Li, Y.; Li, S.; Strong, J.; Neilly, M. B.; Larson, R. A.; Jiang, X.; Zhang, P.; Jin, J.; He, C.; Chen, J. FTO Plays an Oncogenic Role in Acute Myeloid Leukemia as a N(6)-Methyladenosine RNA Demethylase. *Cancer Cell* **2017**, *31*, 127−141.

(28) Zhang, S.; Zhao, B. S.; Zhou, A.; Lin, K.; Zheng, S.; Lu, Z.; Chen, Y.; Sulman, E. P.; Xie, K.; Bogler, O.; Majumder, S.; He, C.; Huang, S. m(6)A Demethylase ALKBH5 Maintains Tumorigenicity of Glioblastoma Stem-like Cells by Sustaining FOXM1 Expression and Cell Proliferation Program. *Cancer Cell* **2017**, *31*, 591−606.e6.

(29) Huff, S.; Tiwari, S. K.; Gonzalez, G. M.; Wang, Y.; Rana, T. M. m(6)A-RNA Demethylase FTO Inhibitors Impair Self-Renewal in Glioblastoma Stem Cells. *ACS Chem. Biol.* **2021**, *16*, 324−333.

(30) Chen, B.; Ye, F.; Yu, L.; Jia, G.; Huang, X.; Zhang, X.; Peng, S.; Chen, K.; Wang, M.; Gong, S.; Zhang, R.; Yin, J.; Li, H.; Yang, Y.; Liu, H.; Zhang, J.; Zhang, H.; Zhang, A.; Jiang, H.; Luo, C.; Yang, C. G. Development of cell-active N6-methyladenosine RNA demethylase FTO inhibitor. *J. Am. Chem. Soc.* **2012**, *134*, 17963−17971.

https://doi.org/10.1021/acs.jmedchem.1c02075
J. Med. Chem. 2022, 65, 10920−10937

(31) Huang, Y.; Yan, J.; Li, Q.; Li, J.; Gong, S.; Zhou, H.; Gan, J.; Jiang, H.; Jia, G. F.; Luo, C.; Yang, C. G. Meclofenamic acid selectively inhibits FTO demethylation of m6A over ALKBH5. *Nucleic Acids Res.* **2015**, *43*, 373−384.
(32) Perry, G. S.; Das, M.; Woon, E. C. Y. Inhibition of AlkB Nucleic Acid Demethylases: Promising New Epigenetic Targets. *J. Med. Chem.* **2021**, *64*, 16974−17003.
(33) Zhou, L. L.; Xu, H.; Huang, Y.; Yang, C. G. Targeting the RNA demethylase FTO for cancer therapy. *RSC Chem. Biol.* **2021**, *2*, 1352−1369.
(34) Wuitschik, G.; Rogers-Evans, M.; Muller, K.; Fischer, H.; Wagner, B.; Schuler, F.; Polonchuk, L.; Carreira, E. M. Oxetanes as promising modules in drug discovery. *Angew. Chem., Int. Ed. Engl.* **2006**, *45*, 7736−7739.
(35) Wuitschik, G.; Carreira, E. M.; Wagner, B.; Fischer, H.; Parrilla, I.; Schuler, F.; Rogers-Evans, M.; Muller, K. Oxetanes in drug discovery: structural and synthetic insights. *J. Med. Chem.* **2010**, *53*, 3227−3246.
(36) Wuitschik, G.; Rogers-Evans, M.; Buckl, A.; Bernasconi, M.; Marki, M.; Godel, T.; Fischer, H.; Wagner, B.; Parrilla, I.; Schuler, F.; Schneider, J.; Alker, A.; Schweizer, W. B.; Muller, K.; Carreira, E. M. Spirocyclic oxetanes: synthesis and properties. *Angew. Chem., Int. Ed. Engl.* **2008**, *47*, 4512−4515.
(37) Burkhard, J. A.; Wuitschik, G.; Rogers-Evans, M.; Muller, K.; Carreira, E. M. Oxetanes as versatile elements in drug discovery and synthesis. *Angew. Chem., Int. Ed. Engl.* **2010**, *49*, 9052−9067.
(38) Carreira, E. M.; Fessard, T. C. Four-membered ring-containing spirocycles: synthetic strategies and opportunities. *Chem. Rev.* **2014**, *114*, 8257−8322.
(39) McLaughlin, M.; Yazaki, R.; Fessard, T. C.; Carreira, E. M. Oxetanyl peptides: novel peptidomimetic modules for medicinal chemistry. *Org. Lett.* **2014**, *16*, 4070−4073.
(40) Ghose, A. K.; Herbertz, T.; Hudkins, R. L.; Dorsey, B. D.; Mallamo, J. P. Knowledge-Based, Central Nervous System (CNS) Lead Selection and Lead Optimization for CNS Drug Discovery. *ACS Chem. Neurosci.* **2012**, *3*, 50−68.
(41) Rankovic, Z. CNS drug design: balancing physicochemical properties for optimal brain exposure. *J. Med. Chem.* **2015**, *58*, 2584−2608.
(42) Wager, T. T.; Chandrasekaran, R. Y.; Hou, X.; Troutman, M. D.; Verhoest, P. R.; Villalobos, A.; Will, Y. Defining desirable central nervous system drug space through the alignment of molecular properties, in vitro ADME, and safety attributes. *ACS Chem. Neurosci.* **2010**, *1*, 420−434.
(43) Wager, T. T.; Hou, X.; Verhoest, P. R.; Villalobos, A. Moving beyond rules: the development of a central nervous system multiparameter optimization (CNS MPO) approach to enable alignment of druglike properties. *ACS Chem. Neurosci.* **2010**, *1*, 435−449.
(44) Svensen, N.; Jaffrey, S. R. Fluorescent RNA Aptamers as a Tool to Study RNA-Modifying Enzymes. *Cell Chem. Biol.* **2016**, *23*, 415−425.
(45) Su, R.; Dong, L.; Li, Y.; Gao, M.; Han, L.; Wunderlich, M.; Deng, X.; Li, H.; Huang, Y.; Gao, L.; Li, C.; Zhao, Z.; Robinson, S.; Tan, B.; Qing, Y.; Qin, X.; Prince, E.; Xie, J.; Qin, H.; Li, W.; Shen, C.; Sun, J.; Kulkarni, P.; Weng, H.; Huang, H.; Chen, Z.; Zhang, B.; Wu, X.; Olsen, M. J.; Muschen, M.; Marcucci, G.; Salgia, R.; Li, L.; Fathi, A. T.; Li, Z.; Mulloy, J. C.; Wei, M.; Horne, D.; Chen, J. Targeting FTO Suppresses Cancer Stem Cell Maintenance and Immune Evasion. *Cancer Cell* **2020**, *38*, 79−96.
(46) Chen, J.; Du, B. Novel positioning from obesity to cancer: FTO, an m(6)A RNA demethylase, regulates tumour progression. *J. Cancer Res. Clin. Oncol.* **2019**, *145*, 19−29.
(47) Xu, D.; Shao, W.; Jiang, Y.; Wang, X.; Liu, Y.; Liu, X. FTO expression is associated with the occurrence of gastric cancer and prognosis. *Oncol. Rep.* **2017**, *38*, 2285−2292.
(48) Yang, Z.; Jiang, X.; Zhang, Z.; Zhao, Z.; Xing, W.; Liu, Y.; Jiang, X.; Zhao, H. HDAC3-dependent transcriptional repression of FOXA2 regulates FTO/m6A/MYC signaling to contribute to the development of gastric cancer. *Cancer Gene Ther.* **2021**, *28*, 141−155.
(49) Kim, H. B.; Lee, H. J.; Kim, G. B.; Lim, H. J.; Park, J. H.; Park, S. G. Clinical Significance of Jagged-1 Activated by APEX1 as a Chemoresistance Factor in Advanced Gastric Cancer. *Anticancer Res.* **2020**, *40*, 1897−1904.
(50) Koosha, S.; Mohamed, Z.; Sinniah, A.; Alshawsh, M. A. Investigation into the Molecular Mechanisms underlying the Anti-proliferative and Anti-tumorigenesis activities of Diosmetin against HCT-116 Human Colorectal Cancer. *Sci. Rep.* **2019**, *9*, 5148.
(51) Zhang, C.; Zhang, M.; Ge, S.; Huang, W.; Lin, X.; Gao, J.; Gong, J.; Shen, L. Reduced m6A modification predicts malignant phenotypes and augmented Wnt/PI3K-Akt signaling in gastric cancer. *Cancer Med.* **2019**, *8*, 4766−4781.
(52) Jacobson, M. P.; Friesner, R. A.; Xiang, Z.; Honig, B. On the role of the crystal environment in determining protein side-chain conformations. *J. Mol. Biol.* **2002**, *320*, 597−608.
(53) Jacobson, M. P.; Pincus, D. L.; Rapp, C. S.; Day, T. J.; Honig, B.; Shaw, D. E.; Friesner, R. A. A hierarchical approach to all-atom protein loop prediction. *Proteins* **2004**, *55*, 351−367.

https://doi.org/10.1021/acs.jmedchem.1c02075
J. Med. Chem. 2022, 65, 10920−10937